Energy Conversion and Management 149 (2017) 61–78

Contents lists available at ScienceDirect

Energy Conversion and Management

journal homepage: www.elsevier.com/locate/enconman

Computational and experimental studies on solar chimney power plants for power generation in Pacific Island countries

M. Rafiuddin Ahmed *, Sandeep K. Patel

Division of Mechanical Engineering, The University of the South Pacific, Suva, Fiji

ARTICLE INFO

Article history:
Received 6 January 2017
Received in revised form 2 July 2017
Accepted 3 July 2017

Keywords:
Solar chimney power plant
Computational fluid dynamics
Solar collector
Experimental testing
Energy storage

ABSTRACT

Computational and experimental studies were performed on solar chimney power plants (SCPP). The first part of the work was optimization of the geometry of the major components of an SCPP of 10 m height and 8 m collector diameter using a computational fluid dynamics (CFD) code ANSYS-CFX to study and improve the flow characteristics inside the SCPP. The collector inlet opening, the collector outlet height, the collector outlet diameter, the chimney divergence angle, chimney inlet opening and the diameter of the chimney were varied and optimum values that give the highest power were obtained. Based on the best configuration achieved for the 10 m high SCPP, a scaled down model of 1:2.5 was modeled and simulated. The 4 m tall SCPP had a collector diameter of 3.2 m. The collector outlet height was kept constant while the collector outlet diameter and the chimney throat diameter were varied in the second part. The collector inlet opening was also varied. The best configuration was then fabricated and extensive experiments were carried out on days of different solar insolations with and without water bags including the effect of atmospheric wind as the third and main part of this work. Detailed measurements of temperature variations along the collector and along the chimney height were performed. The air velocity at the location of turbine was measured and the power available to the turbine was estimated. It was found that, at higher wind speeds, the temperatures along the collector and along the chimney height drop a little; however, the air velocity and available power increase. Water bags were placed under the collector to obtain round-the-clock power. A 100 m SCPP was later modeled and simulated to predict the power available for bigger sized towers at different solar insolations. Such SCPP plants will be very appropriate for Pacific Island Countries; most of these countries have islands with populations of only a few hundred people. Also, the solar insolation is very high in these countries.

1. Introduction

The increasing energy consumption all over the world and the harmful environmental effects of fossil fuels have forced the global energy community to look for renewable sources of power. The demand for electricity is continuously rising especially in developing countries [1]. Unfortunately, fossil fuels are still the primary fuel source and are widely used in most of the countries. For many developing countries, especially the small island developing states (SIDS), a considerable portion of GDP goes towards the cost of fossil fuels. Inadequate energy supplies can not only lead to higher energy costs, but are also a hindrance to the development of a country. With the greenhouse effect and air pollution becoming more severe, utilization of renewable energy sources is increasingly gaining greater importance and playing a major role in solving the above problems [2].

Renewable energy based technologies hold a great promise for the future as they are less harmful to the environment and their resources are available in abundance. Although there are many sources of renewable energy, solar energy is one of the more promising ones since the sun is the ultimate source of most renewable energy supplies. Although solar energy has the highest available energy, only a little fraction of the available energy is used. Solar energy is only available in the day, but technical advancements have made it possible to harness this energy at night by storing the solar energy available in the day [3,4].

A variety of devices have been built to harness solar energy; however most of them are expensive to build and maintain. This is one of the major issues in developing countries. The solar energy device must be simple, reliable and cheap to build and maintain. The Pacific Island Countries (PICs) have limited raw material resources and it is very expensive to import specialized materials.

* Corresponding author.
E-mail addresses: ahmed_r@usp.ac.fj, ahmedm1@asme.org (M.R. Ahmed).

http://dx.doi.org/10.1016/j.enconman.2017.07.009
0196-8904/

So, the preference is for technologies that require cheaper and easily available resources. The solar chimney power plant (SCPP) meets these conditions very well. The SCPP is simple and reliable since it has fewer rotating parts compared to other thermal power plants and it is cheap since the raw materials needed to build an SCPP are readily available in most of the developing countries. The SCPP can also produce power at night by using water bags to store the heat in day time and release this heat slowly at night to provide round the clock power supply [4].

Solar chimney power plants, also called, low temperature power plants, have their working fluid open to the atmosphere. A solar chimney power plant, in its simplest form, consists of three main components [4,5]: the solar air collector, the chimney or the tower and the power conversion unit which include turbines.

The collector is a transparent glass or plastic film close to the ground and is open at the periphery with its height constant, increasing or decreasing towards the center where the chimney is located. Solar radiation enters the collector and gets absorbed by the ground. The chimney is a long cylindrical structure placed at the center of the circular greenhouse collector [6,7]. It is required to ensure an air-tight joint between the collector and the chimney. The air below the collector gets heated up and rises towards the chimney. At the base of the chimney, one or more turbines are placed to extract energy from the rising air which possesses good amount of kinetic energy. Suction from the chimney draws more hot buoyant air from the collector and cold air from free atmosphere replaces the hot air due to natural convection. Water-filled tubes or bags are placed under the collector to make the SCPP work at night. Thus, the solar energy is first converted into thermal energy by the ground, which is then converted into kinetic energy of the hot air and later converted into mechanical energy by the turbine(s) [4,8].

Some of the main advantages of SCPPs compared to other solar thermal power plants include: (a) both direct and diffuse radiation are used for generating power, which is an important factor for PICs where the sky is often overcast, (b) SCPPs are very reliable and are not likely to break down since they have very few moving parts (mainly turbine); the robust structure ensures that very little maintenance is needed, (c) no cooling water is needed which is one of the primary requirements of many power plants [4,9]. This is a major advantage in PICs where the availability of fresh water is an issue, and (d) less developed countries such as PICs can easily build SCPPs as the building materials which are mainly concrete and glass or plastic sheets, are easily available. Also, SCPPs are easy to manufacture and do not require advanced technologies [4,9]. One major drawback of SCPPs is low energy conversion efficiency which means a much larger collector area is required.

2. Background

The concept of an SCPP was conceived as early as 1931 (in [4]). However, the first real concept of an SCPP was proposed by Jorg Schlaich in 1978. In the year 1982, the first (50 kW) SCPP was built and tested for performance in Manzanares, Spain. Haaf et al. [10] presented the principle and construction details of this SCPP while Haaf [11] presented the preliminary test results from this pilot plant. The tower had a height of 194.6 m and a radius of 5.08 m; the mean collector radius was 122 m and the mean roof height was 1.85 m. This plant worked on a regular basis from 1986 to early 1989. It used to start up automatically when the air speed in the tower exceeded about 2.5 m/s. In the year 1987, the mean annual solar insolation was over 150 W/m^2 at the site. Detailed performance of this system, its characteristics, the technical issues and basic economic data for future commercial SCPPs are discussed by Schlaich et al. [4]. Schlaich [12] also provided an overview of SCPPs. During the last decade, there is a tremendous increase in the research works in the area of SCPPs. One of the initial attempts to simulate an SCPP using CFD was made by Bernades et al. [13]. They performed numerical analysis of natural convection in a radial solar heater operating in steady state to predict the thermo-hydrodynamic behaviour of the device. A finite volume method was used to solve the Navier-Stokes and energy equations which gave a detailed picture of the effects of geometric and operational characteristics. The results obtained by Bernades et al. [13] showed that curved junctions initiate well distributed temperature fields and resulted in flow which is free from recirculation as well as a higher mass flow rate compared to straight junctions at the center of the collector. Padki and Sherif [14,15] investigated the viability of SCPPs for medium to large scale power generation and also their viability for rural areas. Detailed theoretical and experimental studies were performed by Pasumarthi and Sherif [7,16] to investigate the performance characteristics of an SCPP. With their mathematical model, they studied the effect of various geometric parameters on the air temperature, velocity and power output of the plant. They then did experimental modifications on the collector: extending the collector base, and introducing an intermediate canvas absorber. The second modification showed more benefits as it increased the air temperature as well as increased the mass flow rate. Their demonstration model had a collector radius of 9.15 m and a chimney height of 7.92 m.

The driving potential of an SCPP was analyzed and the results were presented by Kroger and Blaine [17]. They assessed a number of theoretical models and studied the influence of prevailing ambient conditions. It was found by them that humidified air can enhance the driving potential and at certain conditions condensation may occur. Bernades et al. [5] developed a comprehensive analytical and numerical model to describe the performance of SCPPs. The model was used to estimate the power output of SCPPs and also to study the effect of several ambient conditions and structural dimensions on the power output. They validated the results of their mathematical model against the experimental results and then predicted the performance of large-scale SCPPs. The main conclusions were that the chimney height, the pressure drop across turbine, the size and the optical properties of the collector are the major parameters for a good design of an SCPP.

Ming et al. [18] developed a comprehensive model to evaluate the performance of SCPPs by investigating various parameters like the relative static pressure, driving force, power output and efficiency. They also performed numerical studies to explore the geometric modifications on the system performance based on the Manzanares plant; a good agreement was found with the analytical model. From their work on thermo-economic optimization, Pretorius and Kroger [19] concluded that round-the-clock power generation is possible and the power generation is a function of the collector roof shape and collector inlet height. Pastohr et al. [20] carried out numerical work to study the temperature and flow field in an SCPP. A detailed analysis of the effects of solar radiation on the flow inside the solar chimney plant was performed by Huang et al. [21]. They employed the Boussinesq model and the Discrete Ordinate model for their simulations. They found the pressure throughout the system to be negative; it was also concluded that the temperature difference between the collector inlet and outlet and the pressure difference in the collector-chimney transition section is higher for higher radiation. Ming et al. [22] studied the effect of solar radiation on the heat storage characteristics of the energy storage layer with the help of different mathematical models for different components. Studies were conducted by Koonsrisuk and Chitsomboon [23] based on dimensional analysis together with engineering intuition to combine eight variables into a single dimensionless variable to establish dynamic similarity between a prototype and scaled models of an SCPP. Three plant

configurations were tested numerically for similarity – full geometrical similarity, partial geometrical similarity, and non-similarity. Results obtained from their physical plant were very similar to those of numerical simulations; thus proving the validity of their proposition. It was also found from their studies that for a fixed solar heat flux, different-sized models that have geometric similarity, share an equal excess temperature across the outlet of the collector roof. Studies on the thermal performance of a solar chimney power plant were performed by Ming et al. [24]. A simple analysis of the air flowing through the SCPP was established. Mathematical models for ideal and actual cycle efficiencies for medium- and large-sized SCPPs were developed. Their results provided guidelines for designing and building a commercial-sized SCPP in China.

Zhou et al. [25] carried out a detailed review of the SCPP technology which covered the description of the components, the physical processes, the status of experimental and theoretical studies, the economics of power generation and the new and emerging technologies for solar chimney power generation. Sangi et al. [26] carried out a detailed analysis of an SCPP by performing two different numerical simulations: (a) by solving the Navier-Stokes equations, continuity equation and energy equation numerically using an iterative method, and (b) using the CFD code FLUENT. For the Manzanares prototype, they predicted the temperature, pressure and velocity distributions in the collector for three solar radiations. Their results were in good agreement with the experimental data of the Manzanares plant. Xu et al. [27] developed an axisymmetric mathematical model with the continuity equation, Navier-Stokes equations and the energy equation. They validated their results with the Spanish SCPP results and then presented results of static pressure distribution, velocity distribution, temperature distribution for two turbine pressure drops of 0 Pa and 120 Pa. They also reported results of the influence of solar radiation as well as estimated the energy losses from the canopy and the chimney outlet for these cases. Karatzig [28] carried out a very interesting computer simulation and optimization of the thermo-fluid-mechanical properties of SCPP by developing a one-dimensional model based on flow-tube theory. From his analysis, he reported the temperatures of glass panels, internal air and collector absorber. He also studied the effect of different types of absorbers. He then presented leveled electricity costs and showed that large SCPPs will be very economical especially considering their long life. Fasel et al. [29] performed detailed computational analysis of a number of SCPP models that were geometrically similar to the Manzanares plant using ANSYS FLUENT. They validated their results with a 1:250 scale laboratory model of the Manzanares plant without a turbulence model and concluded that laminar flow assumption is justified at small scale. They also reported the velocity and temperature profiles in the collector and the chimney. They observed strong instabilities for the 1:30 model and suggested that coherent structures embedded in a turbulent flow can be expected for large-scale plants.

Koonsrisuk and Chitsomboon [30] developed a theoretical model of an SCPP and predicted the performance characteristics of large-scale SCPPs; they found that the plant size, the turbine pressure drop and solar heat flux are important parameters that must be carefully chosen for getting optimum output. The velocity and pressure drop of the turbine predicted from their model were slightly lower than the measured values from the Manzanares plant; however, the power extracted by the turbine was almost the same as the measured one. The authors felt that their model, being much simpler than many previous models, would be more useful for future predictions. They proposed an SCPP for Thailand with a height of 400 m and collector radius of 200 m. In another work, the same authors [31] studied the effects of varying flow area by considering combinations of straight and sloping collectors and constant diameter, converging and diverging towers and found that the sloping collector increases the power at the roof entrance. Their main conclusion was that power production can be increased enormously by utilizing a sloping collector and a divergent chimney of (chimney outlet to chimney inlet) area ratio of 16. Gholamalizadeh and Mansouri [32] developed analytical and numerical models to predict the performance of a SCPP in Kerman, Iran. They verified the results from the mathematical model with the actual power from the Kerman pilot plant. They also presented a novel approach to quantify the effect of site altitude with a coefficient called altitude effectiveness. In their work, they also reported the variation of temperature and velocity along the collector. Chan et al. [33] tested a new concept of using a blower to force the air through a divergent chimney until the air flow reaches a steady state and the flow sustains itself thereafter. Li and Liu [34] carried out an experimental study of an SCPP under controlled laboratory conditions at three different heat fluxes of 500, 600 and 700 W/m^2 and used a phase change material for latent heat absorption and release. They found that the discharge period is higher for the latent heat compared to the sensible heat release. Patel et al. [35] carried out a CFD analysis of a 10 m tall SCPP using ANSYS-CFX and studied the effects of inlet opening of the collector, the outlet height of the collector, the outlet diameter of the collector, the chimney divergence angle, chimney inlet openings and the diameter of the chimney. They found the optimum values of the above parameters and concluded that a chimney divergence angle of 2° (each side) gives the best results. Guo et al. [8] felt that the huge opaque chimney blocks part of the radiation and this shadowing effect on the collector must be considered. They simulated an SCPP system and adopted the discrete ordinate model for the radiation, the fan model and the real turbine for pressure drop and performance and used the k-ε turbulence model. They reported the power output, turbine efficiency, collector efficiency, the temperature rise and the updraft velocity for various cases.

In addition to the physical models developed and tested in Manzanares [6,10,11] and by Pasumarthi and Sherif [7], some more experimental models were constructed and tested for performance. In China (Wuhan), an 8 m high SCPP was built with a collector diameter of 10 m [36]. A temperature difference of 24.1 degrees was achieved between the collector outlet and the ambient. A 22 m tall SCPP with a chimney inner diameter of 2 m was constructed in Botswana [37]. A temperature difference of 2–7.5 degrees was recorded depending on the time of the day with the air velocity ranging from 1 m/s to 4 m/s for different cases. The maximum solar insolation reached a maximum of 950 W/m^2 approximately at noon time. In Brazil [38], an SCPP of 11 m height and 25 m collector diameter was constructed. The collector had a height of 0.5 m and was made of a plastic film supported by a steel structure. A 4 m high SCPP model with a tower diameter of 0.32 m and a 3 m collector was tested in a laboratory experiment by Motoyama et al. [39]. The main objective was to assess the increase in wind velocity inside a diffuser type tower compared to the cylindrical type tower. It was found that the velocity inside the diffuser tower is almost 1.5–1.8 times higher compared to the constant diameter tower for a temperature difference of 20–35 degrees without a turbine. Lee et al. [40] designed a 1.9 m tall solar chimney which acted as a collector to supply heat to an organic Rankine cycle plant. They varied the chimney tilt angle and length and studied the outlet temperature. Maghrebi et al. [41] developed a mathematical model of a sloped SCPP and validated the results from the model with experimental results. Semai et al. [42] computationally studied the effect of slope of the collector inlet on the performance of a SCPP. They found that the configuration with converging flow towards the collector center gave the best performance. Larbi et al. [43] studied the performance of SCPPs with mathematical model, experimental work and theoretical analysis

for the south-western region of Algeria. They studied the effect of geometric parameters on the performance of SCPP. They also studied the effect of atmospheric wind and found that higher wind speed reduces the power production. Okoye and Taylan [44] carried out a performance analysis of a SCPP for the rural areas in Nigeria. Their studies were carried out for a number of locations with different solar insolations. They carried out a substantive sustainability analysis considering the three inter-related dimensions of social, economic and environmental aspects. They concluded that SCPP can enhance the energy access in the rural areas of Nigeria. Okoye et al. [45] proposed an approach to simultaneously determine the optimal dimensions of the SCPP and the economic feasibility of the plant. Guo et al. [46] built an indoor SCPP and measured the airflow temperature and updraft velocity for different insolations and chimney heights. Ming et al. [47] presented a review of the developments in the area of SCPPs. They also studied the effect of providing radial partition walls distributed uniformly under the collector canopy and found it advantageous. They also studied the effect of ambient cross-wind on the output of the SCPP and found that a collector with a higher inlet shows a deterioration in the performance that is more significant compared to a collector with a lower inlet. They concluded that a divergent chimney provides a higher mass flow rate through a SCPP; an observation also reported by Koonsrisuk [48], Ghorbani et al. [49] and recently by Hu et al. [50]. Hu et al. [50] performed studies for divergence angles of 0° to 6.8° and concluded that larger divergence angles reduce the temperature rise in the collector which counteracts the enhancement effect from the pressure recovery of the divergent SCPPs, affecting power output adversely. Ali [51] performed a techno-economic optimization of SCPPS. He considered three designs: reinforced concrete chimney, sloped collector and floating chimney. The SCPP with floating chimney showed shorted payback periods and the optimized design showed significant cost savings for the same power output. Ayadi et al. [52] carried out experimental and numerical studies on the effect of collector roof inclination on the performance of an SCPP. They reported distributions of velocity, temperature, pressure, incident radiation and turbulent kinetic energy. They observed that a divergent collector with a cylindrical chimney gives better performance. Shirvan et al. [53] carried out an optimization of effective parameters on an SCPP to achieve maximum power. They also performed a sensitivity analysis with input parameters of collector gap, tower diameter and tower height as well as the inclination of collector. The obtained and presented optimized configurations for potential maximum power enhancement due to the increase in the tower diameter and due to the increase of the tower height.

The present work briefly discusses the main findings from our previous work on a 10 m tall SCPP [35] based on which further simulations were performed on a scaled down model of 4 m height and the best configuration was then fabricated and tested under real conditions. The ground temperature (under the collector) recorded at about 2.00 pm in the first week of December 2013, when the solar insolation was slightly above 600 W/m^2, was used as an input parameter for both the 10 m and 4 m tall towers. Geometric parameters were varied for both the 10 m and 4 m high SCPPs to study and improve the flow characteristics and the available power; thus obtaining the best configurations was the main aim of the computational work. The experiments on the best configuration of the 4 m high SCPP were performed on days of different solar insolations in 2013 and 2016 with and without water bags. The effect of atmospheric wind on the temperatures and on the air velocity and available power at the turbine section was studied. Detailed measurements of temperature variations along the collector and along the chimney height were performed at different solar insolations. The effect of water bags on the temperatures, air velocity and power is studied and fluctuations in power with water bags are discussed. Since the present work itself became enormous, the plan to install a turbine was postponed for future work and the attention is focused on understanding the thermo-fluid mechanics of the experimental SCPP.

3. Computational work

ANSYS-CFX Ver. 14 was used for simulation purpose in this work. It uses unsteady Navier-Stokes equations in their conservation form. The equations are presented in Ref. [35]. CFX Ver. 14 can model natural and mixed convection flows by the inclusion of buoyancy source terms. Natural convection flows occur when the convection of a fluid is driven only by local density variations while mixed convection flows occur when the convection of a fluid is driven by both a pressure gradient and buoyancy forces.

3.1. Modeling and meshing of the 10 m high SCPP

Autodesk Inventor was used to create the model of the SCPP as shown in Fig. 1. The SCPP model consisted of two major components, the solar chimney and the solar collector. The overall height of the SCPP was 10 m and the collector diameter was 8 m. A diverging collector was used due to its superior performance compared to a horizontal or a convergent collector [31,54]. Three collector outlet height of 0.5 m, 0.75 m and 1 m, two collector outlet diameters of 0.6 m and 1 m, and two chimney throat diameter of 0.25 m and 0.3 m were modeled and tested. The collector inlet opening was varied from 0.05 m to 0.2 m in increments of 0.05 m and the chimney divergence angle (each side) was varied from 0° to 3° in increments of 1°. The different combinations resulted in more than 190 sets that were all tested computationally [35].

Grid generation was done using ANSYS ICEM CFD software. The domain was discretized using the ICEM CFD Hexa-mesher or user-defined meshing method. The hexahedral grid ensures that the results obtained are of the highest quality and accuracy. Meshing for the solar chimney is shown in Fig. 2. The total number of nodes for the model was 157,432. A grid independence test was performed with three grid sizes and it was found that increasing the number of nodes to 904,392 resulted in only a difference of 1% in the mass flow rate. Hence, the simulations were performed with 157,432 nodes [3,35].

Fig. 1. The SCPP model created in Autodesk Inventor.

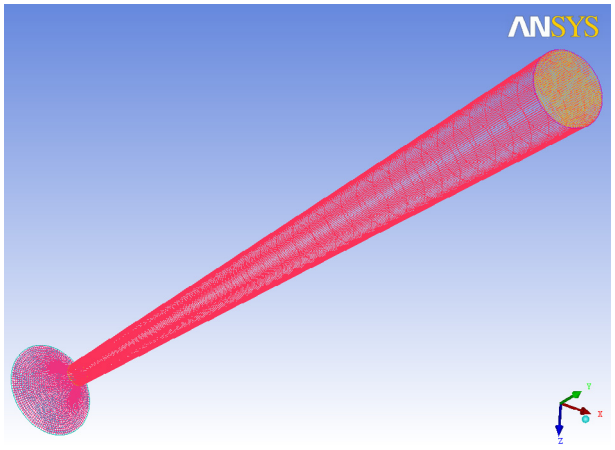

Fig. 2. The solar chimney mesh [35].

ANSYS CFX is a Reynolds Averaged Navier-Stokes Equation (RANSE) solver based on finite volume technique. Steady state analysis was chosen for the simulations. Air (as an ideal gas) was the working fluid. The model was built from the origin and extended in the positive *y*-direction. The buoyancy model was then activated by specifying the gravity of –*g* in the *y* direction which represented real life flow. The reference pressure was 1 atm. Full buoyancy model was chosen in CFX to account for the changes in density and the effect of buoyancy. For single phase flows, this model is used when temperature and pressure variations directly affect the fluid density. These include all ideal gases and real fluids. In most gases, temperature variations significantly affect densities, hence this model is appropriate. For turbulence Modeling, the SST (shear stress transport) model was used; this model is a hybrid two-equation model that combines the advantages of both k-ε and k-ω models. The k-ω model performs much better than k-ε models for boundary layer flows and gives better results in cases involving boundary layers under adverse pressure gradients [55]. The heat transfer model selected was total energy, as the variation in kinetic energy is also of significant importance in addition to the changes in temperature. The boundary types at the inlet as well as the outlet were set to openings with boundary conditions of zero relative pressure and a static temperature of 303 K. The ground (absorber) was assigned a no-slip wall condition with its temperature 323 K. This was based on the measurement of the ground temperature when the solar insolation was 607.8 W/m^2. The remaining sides of the domain were modeled as no-slip walls. Automatic mesh connection method was selected for the interface. The simulation was run for 5000 iterations; for convergence, residual type of root-mean-square (RMS) and the residual target value of 1×10^{-7} were set as the criteria.

3.2. Modeling of the 4 m high SCPP

As mentioned above, another SCPP model with an overall height of 4 m and collector diameter of 3.2 m was simulated as the second part of this work. The divergence angle was kept the same as for the 10 m tower at 2° (each side) as it was found to be the optimum for the 10 m tower. The height of the collector outlet was kept constant at 0.2 m. The collector outlet diameter, the collector inlet opening and the chimney throat diameter were varied. The collector inlet opening was varied from 0.02 m to 0.08 m at increments of 0.02 m. These are important parameters which need to be selected carefully for every SCPP [19]. Directly scaling them from another model may not give the best results. The collector outlet diameter and the chimney throat diameter were varied as shown in Table 1. All these cases were tested with all the collector inlet openings.

4. Experimental method

A 4 m tall SCPP was constructed for experimental purpose. The overall dimensions of the SCPP are shown in Fig. 3. The components of the SCPP were fabricated individually in the Engineering Workshop of the University. A 1.6 mm thick galvanized sheet metal was rolled into a cone shape for the chimney. Three different sections of 1200 mm each were separately manufactured and welded together to complete the 3600 mm tall chimney. The total height of the SCPP was 4 m. Extreme care was taken to fabricate the bellmouth as it is one of the main components of the SCPP which ensures smooth flow from the collector to the chimney. The fabricated bellmouth was then welded to mild steel flanges and the inner diameter of the flange was tapered to exactly match the profile of the inner radius of the bellmouth. A 'Bondo' brand body filler (plastic filler containing 11–18% Styrene mixed with Dibenzol Peroxide hardener) was used to fill any small gaps and to smoothen the inner surface.

The frames of the collector were made of 40 mm × 40 mm × 1.6 mm galvanized steel square tubing. This was done to provide structural stability as the collector has to withstand the weight of 6 mm Perspex and the weight of the people who need to walk on the collector during assembly and testing. To secure the components together, eight M16 high tensile bolts were used. Fig. 4 shows a three-dimensional view and the schematic of the frames of the solar collector.

Three 5 mm diameter galvanized steel guy wires were attached to the chimney top and secured at angles of 120° on the ground using augers. The foundation of the plant was 1 m deep. A schematic diagram of the foundation and the footing details are shown in Fig. 5, while a photograph of the completed 4 m tall experimental SCPP is shown in Fig. 6.

PT–100 temperature sensors were used to measure the temperature along the collector and along the chimney height, as shown in Fig. 7. The PT–100 temperature sensors have a measurement range of −200–400 °C, with a resolution of 0.1 °C. The accuracy of temperature measurements with the PT-100 sensor is ±0.5%. The initial temperature data were logged and stored using a Daq-PRO data-logger. This data-logger is a portable battery-operated system with 8-channel data-logging capabilities and an accuracy of ±0.5%. A Chromel-Alumel type K thermocouple having a measurement range of −200 °C to 1260 °C and a Center-305 data-logger thermometer was also used for temperature measurements. The thermocouple has an accuracy of ±0.75%. Provisions were also made on other sides of the collector to make temperature measurements. The temperature measurements performed during phases/days of sustained winds of 2 m/s or greater were either not recorded or discarded (except for Section 5.3). It was also ensured that the measurements reported here are performed in the absence of significant variations during the measurement time-span. A pitot static tube was fitted a little above the throat of the chimney for finding the velocity of air at the throat. The pitot static tube was aligned such that it reads the maximum total

Table 1
Different configurations of the 4 m SCPP tested.

Cases	Collector outlet diameter (m)	Chimney throat diameter (m)
A	0.24	0.10
B	0.4	0.10
C	0.24	0.12
D	0.4	0.12

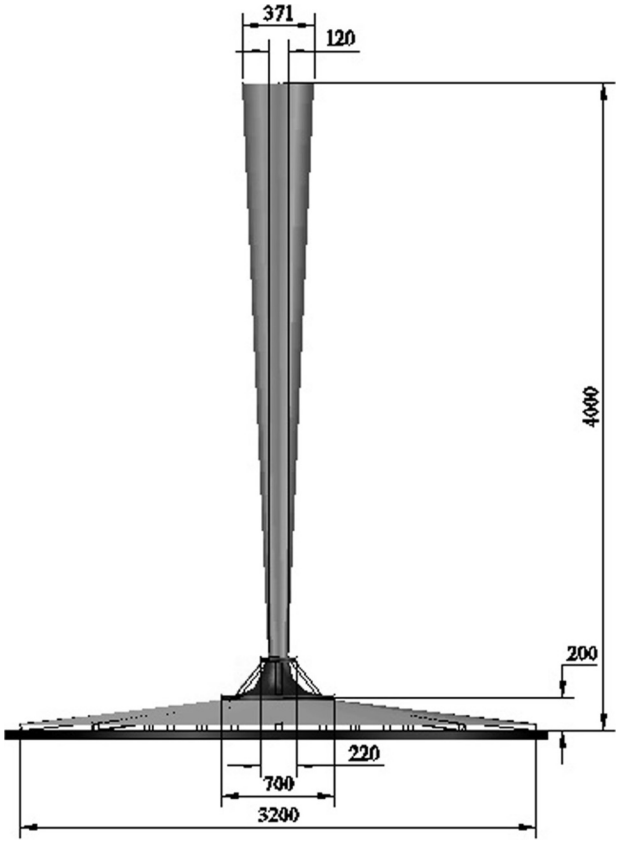

Fig. 3. Schematic diagram of the 4 m tall experimental SCPP (dimensions in mm).

pressure to ensure that it is perfectly parallel to the flow. The pressures were measured using a Furness Controls FCO510 digital micromanometer which communicated the data to a Windows laptop using RS232 communication or averaged and logged in the micromanometer during the measurement span. The digital micromanometer has a range of −2000 to +2000 mm of water. The accuracy of pressure measurements with this micromanometer is ±0.25%. The solar insolations were measured with a Licor LI200S Pyranometer that has a maximum deviation of 1% up to 3000 W/m^2 and a cosine correction up to 80° angle of incidence. The absolute maximum error in solar insolation measurements with this Pyranometer is ±5% with a typical error of ±3%.

The accuracy of velocity measurements was estimated following the procedure of Moffat [56]. The velocity V is calculated using the values of water density, air density and the differential pressure Δh (from the total and static pressures) using the relation from Bernoulli's equation

$$V = \left[2\frac{\rho_{water}}{\rho_{air}} g\Delta h\right]^{0.5} \quad (1)$$

Taking the density of water and g as constants, the percentage error in the estimation of velocity is obtained as

$$\frac{dV}{V}\times 100 = \pm\frac{1}{V}\left[\left(\frac{\partial V}{\partial \rho_{air}}\right)^2 (d\rho_{air})^2 + \left(\frac{\partial V}{\partial \Delta h}\right)^2 (d\Delta h)^2\right]^{0.5} \times 100 \quad (2)$$

The maximum error in the estimation of velocity is thus estimated to be 4.9%.

5. Results and discussion

5.1. SCPP of 10 m overall height

The results are presented and discussed in this section. In this section, only some of the results from the computational studies on the SCPP of 10 m height and 8 m collector diameter will be presented. For all the results, the readers are encouraged to read

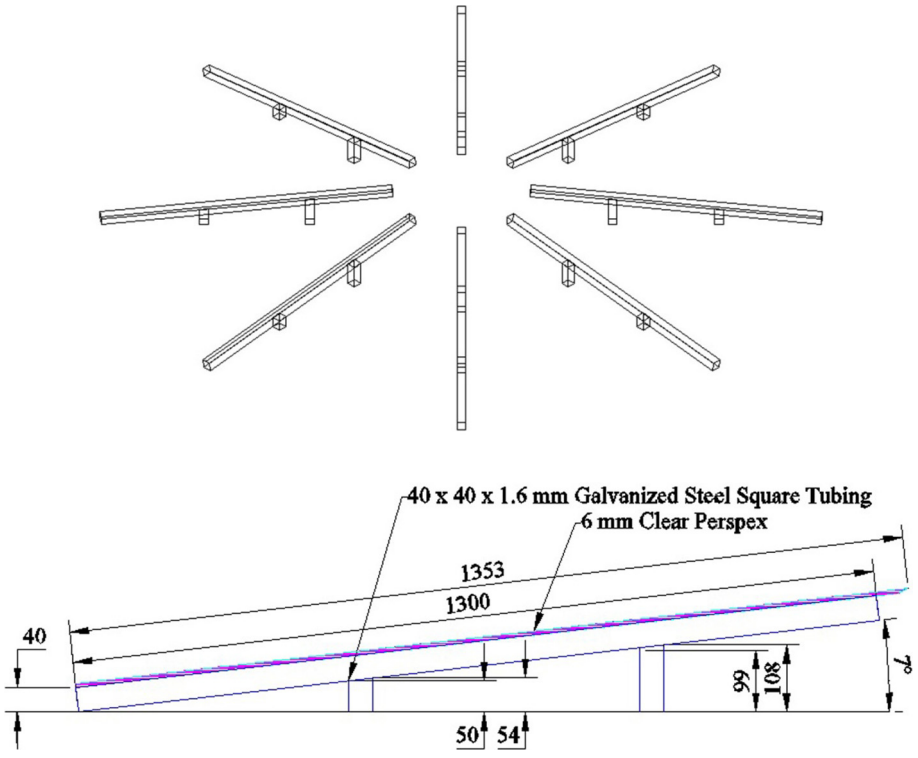

Fig. 4. Three-dimensional view and schematic of the frames of the solar collector.

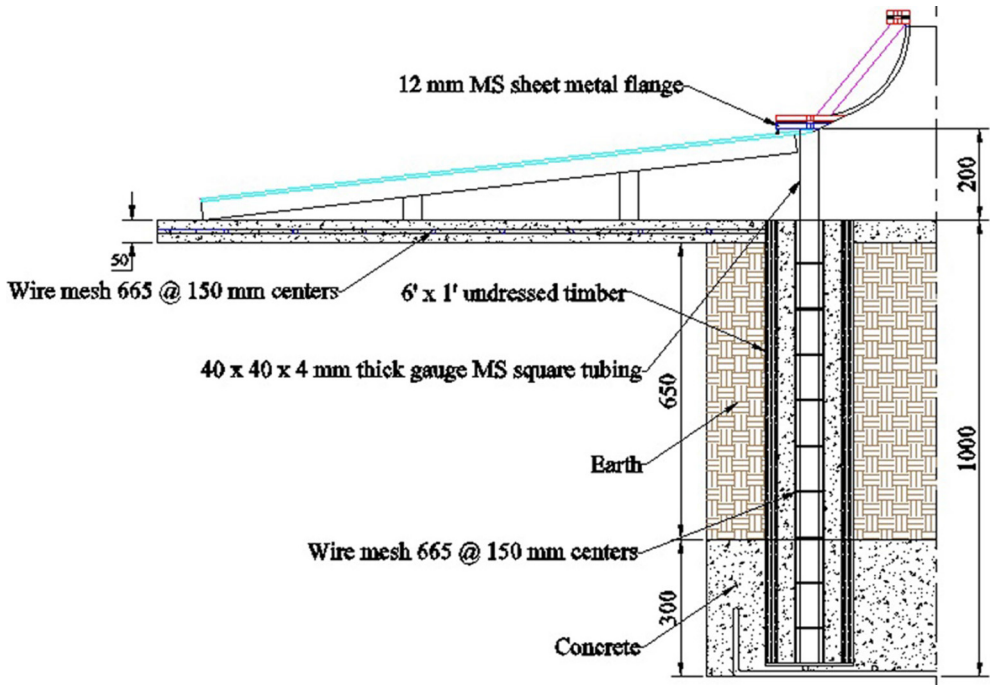

Fig. 5. Schematic diagram of the foundation and footing.

Fig. 6. A photograph of the 4 m tall SCPP built in Suva, Fiji.

Ref. [35]. The optimum parameters obtained from all the simulations (more than 190) are presented here. The collector outlet height, outlet diameter, and the chimney throat diameter were varied along with the collector inlet opening and the chimney divergence angle (depicted in Fig. 8), as described in Section 3.1.

The power available to the turbine was calculated using:

$$P_{available} = 0.5\rho AV^3 \quad (3)$$

where ρ is the air density, A is the area and V is the air velocity at the measurement point.

The power available was calculated at the measurement location, shown in Fig. 7 and Fig. 8. Fig. 9 shows the power available for various collector inlet openings for a collector outlet height of 0.75 m, collector outlet diameter of 0.6 m and chimney throat diameter of 0.25 m for the four chimney divergence angles. For the opening of 0.05 m, the power available was the highest while it was the lowest for the 0.2 m opening. At the divergence angle of 2°, the power peaked for most of the inlet openings [35]. It is clear that SCPPs with divergent chimneys produce more power compared to the constant diameter chimneys. This is because of the increase in the mass flow rate due to a reduced frictional resistance. The frictional head loss is directly proportional to the square of velocity and inversely proportional to the diameter at that section. The static pressure measurement at the chimney throat section indicated that the pressure is less than atmospheric there. The highest velocity and the lowest pressure at the chimney throat section due to the area being the smallest resulted in a considerable flow modification in the divergent section with the pressure rising to meet the atmospheric pressure at the chimney outlet at the expense of the kinetic energy of the air. It can be seen from Fig. 12 in the next section that the velocity reduces drastically to allow the pressure to recover to meet the atmospheric pressure at the outlet. It can be seen that the velocity becomes half of the maximum velocity in a very short distance from the throat; thus the reducing velocity in the divergent section resulted in a significantly reduced power loss due to much lower system resistance. Similar observations were made by a number of researchers who found that a divergent chimney produces more power compared to a constant diameter chimney [31,39,48–50]. Koonsrisuk and Chitsboon [31] reported an increase in power output of nearly 180 times for the divergent chimney compared to the straight chimney. Okada et al. [57] reported a velocity increase of 1.38–1.44 times and power increase of 2.6–3.0 times for the 4° divergent chimney compared to the cylindrical chimney. Higher values of available power for the lower openings are due to the very little interaction of the heated air inside the collector with the ambient, creating a very effective heating area under the collector. Also, since there is less air inside the collector for the smallest opening,

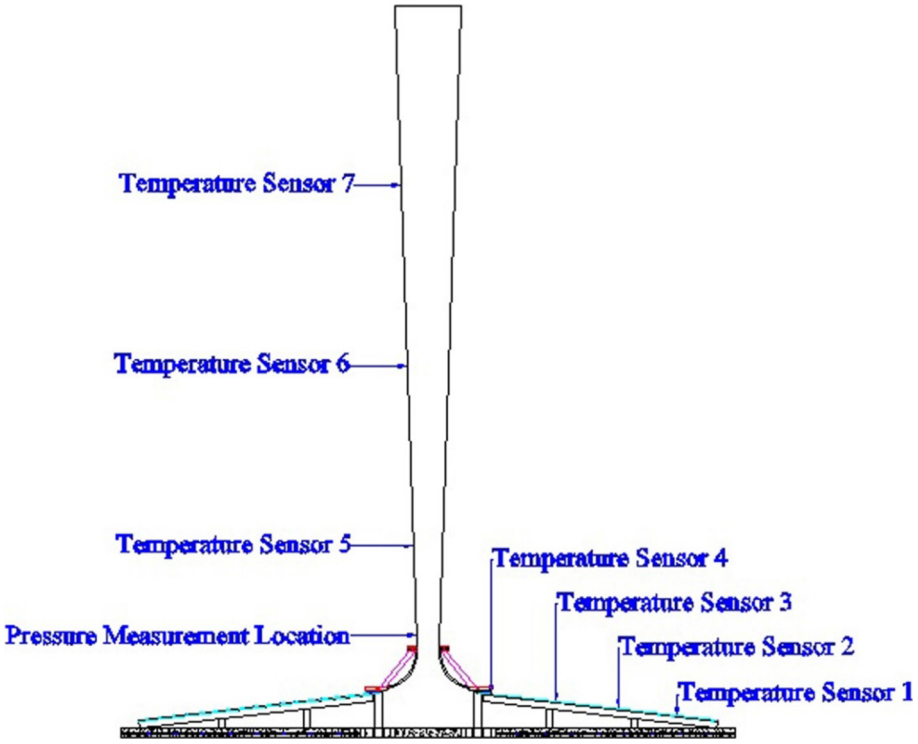

Fig. 7. Locations of temperature and pressure sensors.

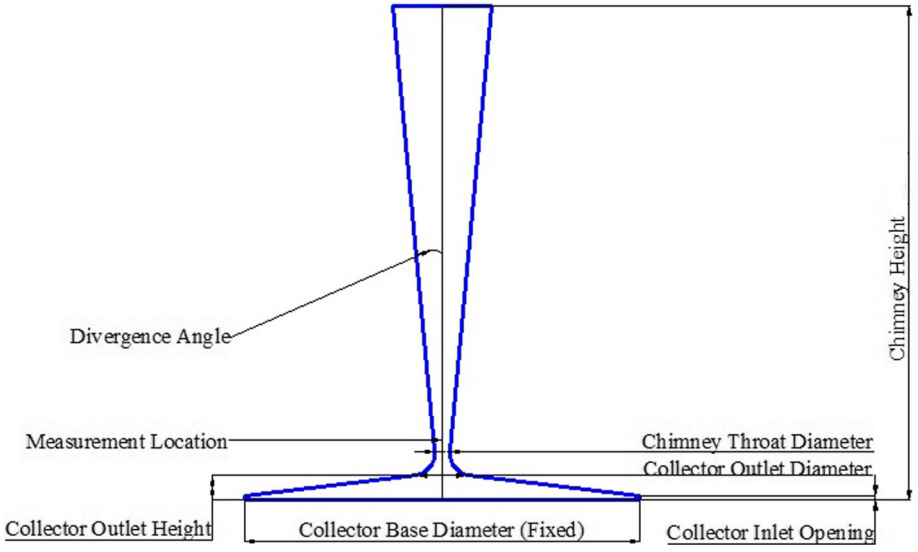

Fig. 8. Various parameters of SCPP that were varied.

it stays for a less time inside the collector; it heats up faster and rises through the chimney.

Based on the more than 190 simulations performed, the best configuration having a collector inlet opening of 0.05 m, a collector height of 0.5 m, a collector outlet diameter of 1 m, a chimney throat diameter of 0.25 m with a divergence angle of 2° was chosen, as it gave the maximum power [35]. The velocity for this case increased sharply to a height of 1 m due to the nozzling effect, reaches a maximum of 7.86 m/s at the turbine section and then decreases in the diverging section. The maximum available power is 14.5 W for this case. Along the collector radius, the temperature increased sharply and reached about 322 K at a height of 0.025 m above the ground [35].

5.2. Computational results for the 4 m tall SCPP

The powers available as a function of collector inlet opening for the four cases A, B, C and D are shown in Fig. 10. The highest available power of 0.57 W was achieved for case B for the smallest collector inlet opening of 0.02 m. However, Case D recorded higher power for most of the collector inlet openings except for 0.02 m. Thus it can be seen that the smallest collector inlet opening of 0.02 m has the highest available power in almost all the cases and the reason for this is already discussed in the previous section. The mass flow rate will be higher for the smaller openings; this is enhanced for larger collector outlet diameters as they accommodate and allow the heated air from the entire collector to rise

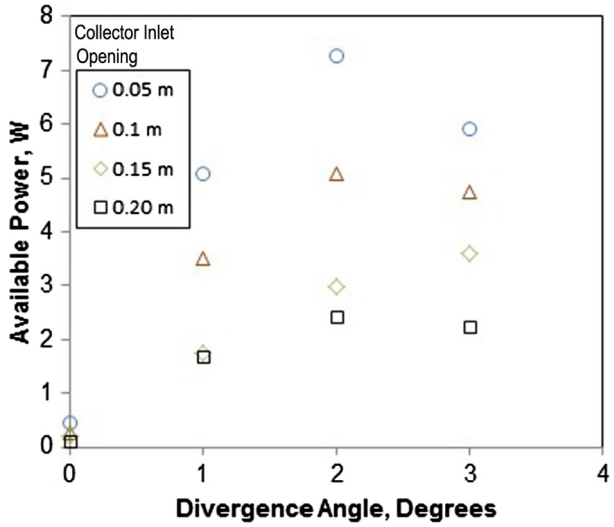

Fig. 9. Power available for various collector inlet openings and chimney divergence angles for a collector outlet height of 0.75 m, collector outlet diameter of 0.6 m and chimney throat diameter of 0.25 m [35].

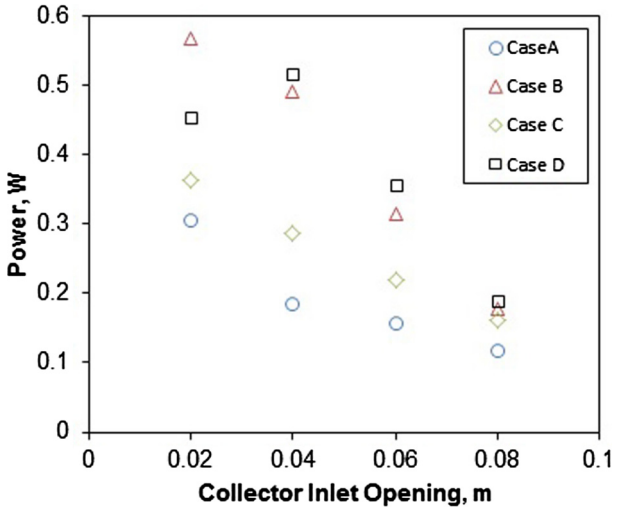

Fig. 10. Power available for cases A, B, C and D as a function of collector inlet openings for the chimney divergence angle of 2°.

and flow faster. For this reason, cases B and D exhibit higher powers compare to other cases. For case B, the nozzling effect from the collector outlet to the chimney throat is higher as the throat diameter is smaller in this case. This may give rise to flow acceleration from the collector outlet to the throat, resulting in higher velocity and available power (which is proportional to the cube of velocity) at the throat.

Fig. 11 shows the mass flow rate for all the different configurations of the 4 m SCPP. It can be clearly seen that the highest mass flow rate of 0.063 kg/s was achieved for case D for the collector inlet opening of 0.04 m. Case D recorded the highest mass flow rate for all collector inlet openings. The collector inlet opening of 0.02 m has the highest mass flow rate in almost all cases and the collector inlet opening of 0.10 m has the lowest mass flow rate among all the cases except for case D where the highest flow rate was achieved at a collector inlet opening of 0.04 m. The larger collector outlet diameter of 0.4 m had higher mass flow rate compared to the smaller collector outlet diameter of 0.24 m having the same chimney throat diameter in all respective cases. It can

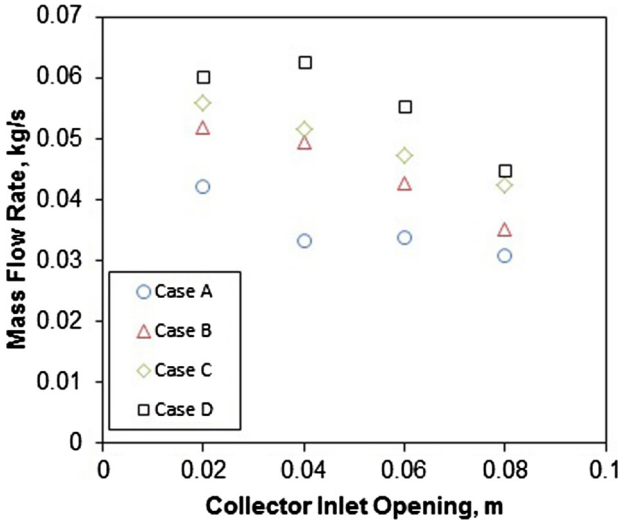

Fig. 11. Mass flow rates for cases A, B, C and D for the chimney divergence angle of 2° and different collector openings.

also be noted that chimney throat diameter of 0.12 m had higher mass flow rate compared to chimney throat diameter of 0.10 m for almost all collector inlet openings.

The maximum air velocities at the chimney throat for all the cases are shown in Fig. 12. The highest velocity of 4.67 m/s was recorded for case B when the collector inlet opening was 0.02 m. In fact, for all the collector inlet openings, case B achieved higher velocities. Interestingly, the highest velocity for almost all the cases was recorded for the collector inlet opening of 0.02 m. For the highest collector inlet opening, the lowest velocities were recorded except for case D. Higher velocity was achieved for the larger collector outlet diameter of 0.4 m compared to that of 0.24 m for the same chimney throat diameter. Overall, cases B and D recorded higher velocities for the reasons explained earlier. However, since the throat area is higher for case C, it gave a slightly higher mass flow rate than case B (Fig. 11). It should also be noted that the pressure, temperature and density are different at the throat for different cases due to changes in the geometric parameters. The density will be higher for cases C due to the convergence of flow into a smaller collector outlet area compared to case B,

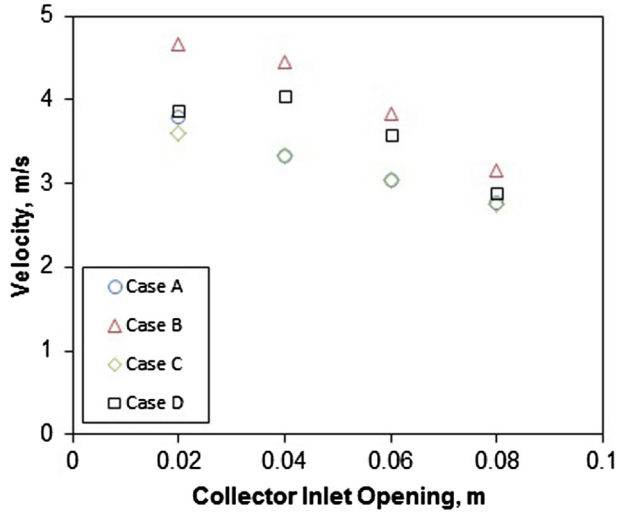

Fig. 12. Velocities for cases A, B, C and D as a function of collector inlet opening for the chimney divergence angle of 2°.

resulting in a higher mass flow rate. For case D, the throat area is larger than case B, resulting in a higher mass flow rate for this case.

Based on the above simulation results, case D with a collector inlet opening of 0.04 m was selected for experimental testing due to the high mass flow rate, high maximum velocity and hence high available power (partly also because a collector opening of 0.02 m around the collector is difficult to achieve and maintain practically). It should be noted that optimum values of other parameters, from the range of those values, were already obtained in the first part of this work; however, it was checked that for case D, the 2° divergence angle gives a higher velocity than the 'scaled down' velocity from the 10 m high SCPP to 4 m high SCPP, ensuring that our scaled down model gave the best performance. Fig. 13 shows the velocity vectors for case D from CFD. It can be seen that the highest velocity of 4.05 m/s is recorded slightly above the chimney throat. Shahreza and Imani [58] recorded a velocity of 5.12 m/s in their innovative SCPP of a total height of 2.6 m, which had two intensifiers to increase the heat transferred to the collector along with an air tank downside of the system to absorb the increased radiation. For their 2 m tall experimental SCPP, Motoyama et al. [39] measured a maximum velocity of 3 m/s for a temperature difference of 20 degrees. Fig. 14 shows the temperature contours on the entire model for the collector inlet opening of 0.04 m. The highest temperature can clearly be seen at the ground. The temperature is lower at the inlet to the collector and starts to rise towards the center. Higher temperatures can clearly be seen near the center of the collector. It can be seen that the temperature increases towards the center of the collector as the hot air moves through the bellmouth to the chimney. The temperature drops a little along the height of the chimney. The temperature rise from the collector inlet to the center is about 12 degrees; Pasumarthi and Sherif [14] from their experimental tower of 7.92 m height and collector radius (unextended) of 4.57 m recorded a temperature rise of about 9 degrees for a solar insolation of 700 W/m^2 and about 10 degrees for an insolation of 800 W/m^2.

5.3. Experimental results for the 4 m tall SCPP

For validating the computational results, comparison of the temperature variation from the collector inlet to the center and along the chimney height were made. The air velocity in the chimney was also compared at different locations along the height. To get an idea of the variation in the solar insolation during the day, measurements of solar insolation performed over three typical days in December 2013 were averaged and plotted; the ambient temperature was also plotted as a function of time as can be seen from Fig. 15. The maximum solar insolation was, almost always, recorded at 1.00 pm. The maximum average ambient temperature of 302.5 K was also recorded at 1.00 pm. The maximum temperature among the three days (304.5 K) was also recorded at 1.00 pm. It should be noted that the largest variation in the ambient temperature from the three-day average was only about 2 degrees, while the solar insolation varied by 184 W/m^2 at the same time (3.00 pm).

Initial measurements at the same solar insolation which gave the ground (absorber) temperature of 323 K showed a difference of 0.5–2 degrees between experimental and computational results, with the difference being larger near the collector inlet. The experimental temperatures were generally higher than computational. It was found that this was due to the temperature sensors being very close to the ground (absorber), where the temperature is higher. Later experiments conducted by moving the sensor upwards from the ground to the collector showed an interesting temperature profile. The temperature measurements were performed from the ground to the collector lower surface in increments of 22 mm at the sensor location 3 of Fig. 7 and the results are shown in Fig. 16 (h is the height of the sensor tip above the ground and H is the height of the collector from the ground). The solar insolation at the time of measurements was about 700 W/m^2. It can be seen that the temperature drops sharply from the ground to the first measurement point; it continues to decrease and then increases at the collector lower surface. The mean air temperature is recorded halfway between the ground and the collector. All subsequent measurements were performed at this height to ensure the correct air temperature.

Fig. 17 shows the comparison between the computational and experimental temperatures from the collector inlet to the collector outlet (sensor numbers 1–4). It can be seen that the maximum temperature difference is near the inlet to the collector (sensor number 1). The experimental temperatures are generally higher than the computational temperatures; however, at the location closest to the collector outlet, the experimental temperature is

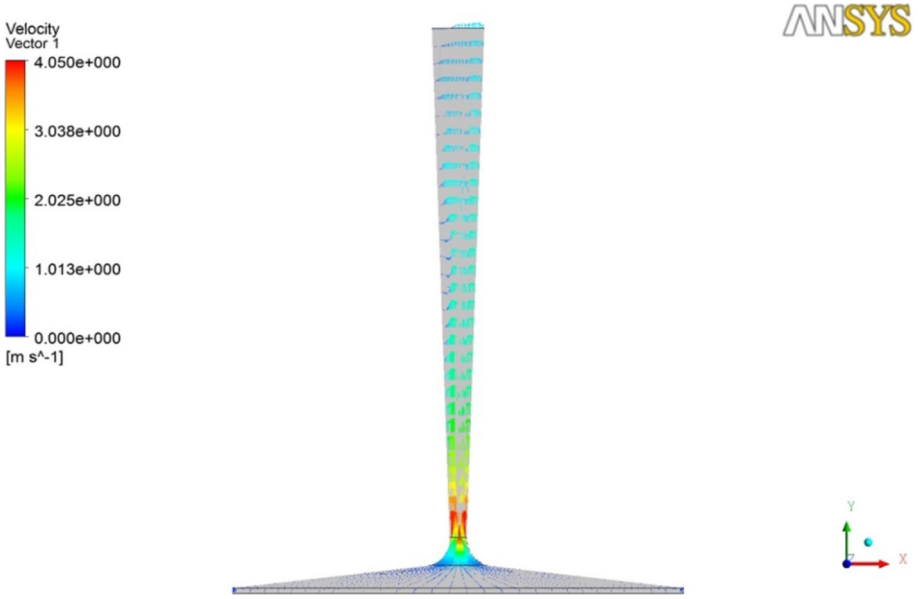

Fig. 13. Velocity vectors on the entire SCPP for case D for the collector inlet opening of 0.04 m.

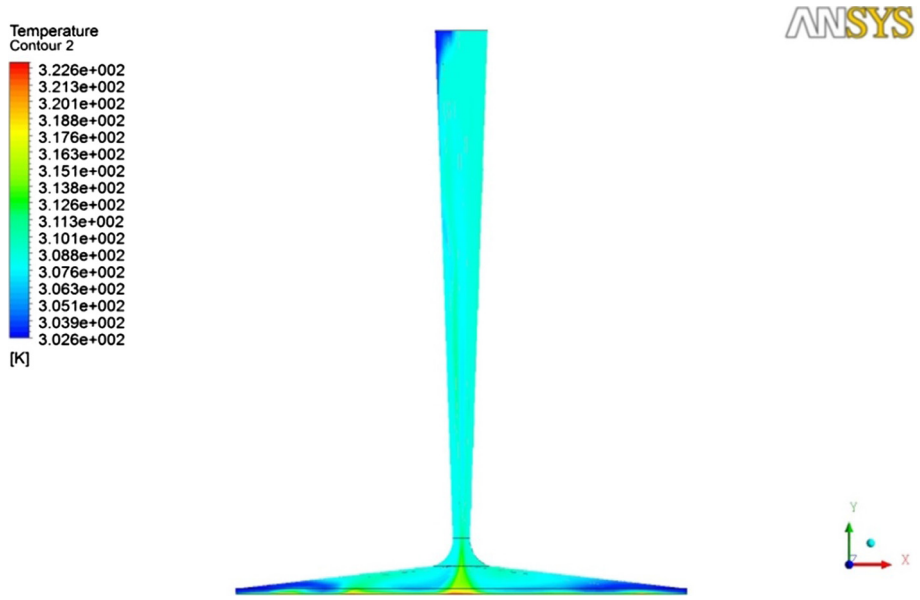

Fig. 14. Temperature contours on the entire model for case D. The collector inlet opening is 0.04 m.

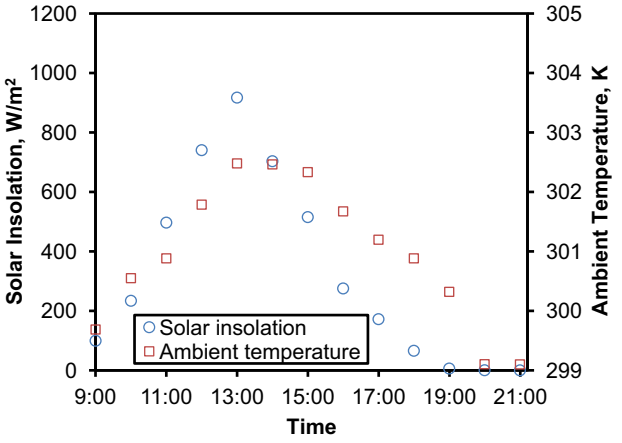

Fig. 15. Variations of solar insolation and ambient temperature averaged over three days in December 2013. The maximum deviation in solar insolation from the averaged values was 184 W/m^2 and that in the temperature was 2 K.

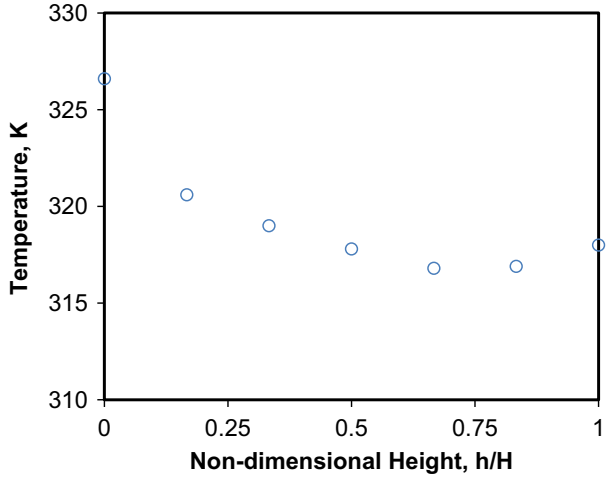

Fig. 16. Temperature variation from the ground to the collector lower surface when the solar insolation was 700 W/m^2.

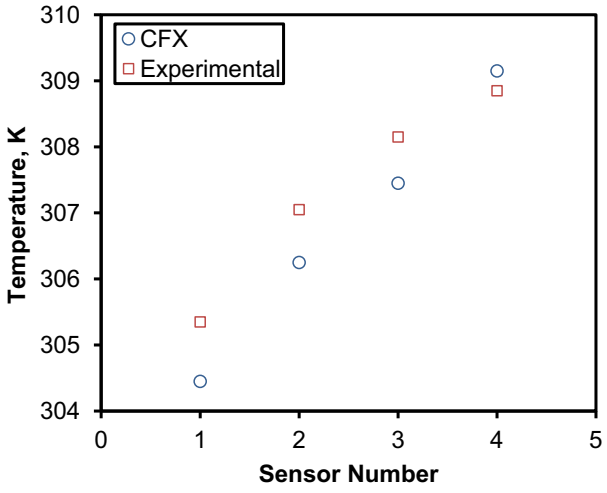

Fig. 17. Temperature variation from the collector inlet to the center obtained from experimentation and computations for case D for the collector inlet opening of 0.04 m.

slightly lower. It should be noted that the maximum temperature difference is less than 1 degree. For the purpose of validating computational results, the experimental measurements recorded only in the absence of cross-wind were considered. For this purpose, the thermocouple was also used for making temperature measurements.

Another comparison of temperature variation along the height of the chimney was made between experimental and computational results and the results are shown in Fig. 18. It can clearly be seen that the maximum difference is less than 1 degree for all of the cases validating our CFX results. It should also be noted that the main purpose of the computational work was to obtain the best configuration to perform detailed experimental measurements.

Most of the detailed measurements were performed in 2016 and the hourly variations of ambient temperature and solar insolation from 9.00 am to 9.00 pm, averaged for three typical days in February, when a number of measurements were performed, are shown in Fig. 19. The average solar insolation at 1.00 pm exceeded

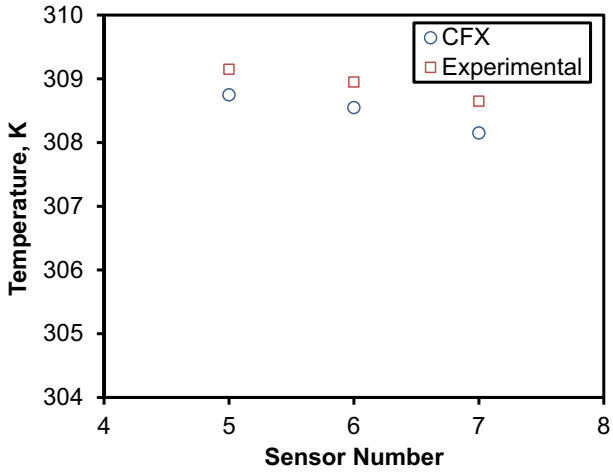

Fig. 18. Temperature variation along the chimney height obtained experimentally and computationally for case D. The collector inlet opening is 0.04 m.

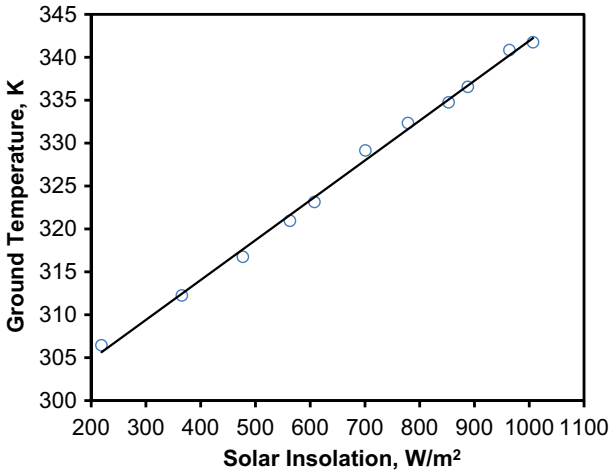

Fig. 20. Variation of ground (absorber) temperature with solar insolation.

1000 W/m^2; the average ambient temperature at this time was 304 K. However, the maximum average temperature was recorded at 3.00 pm (also the maximum in a day). It is worth noting that although the temperature was higher at 3.00 pm, the solar insolation still peaked at 1.00 pm. The sunset time in February is around 6.45 pm, hence the solar insolation at 7.00 pm was almost zero.

Considering the wide range of solar insolations occurring during the measurements, it was decided to study the variation of the ground (absorber) temperature at different insolations. Fig. 20 shows the increasing ground temperature under the collector at increasing solar insolations. It can be seen that the variation of ground temperature with solar insolation is almost linear. A best fit straight line was drawn and its equation was obtained to be

$$y = 0.0464x + 295.47 \quad (4)$$

This equation was found to be very interesting on examination. When the effect of solar heating totally disappears (5.00 am to sunrise) and the earth's re-radiation is the least (when $x = 0$), the ambient temperature falls to its minimum [59]; from our measurements, the minimum temperature was around 296 K (23 °C) during the months when most of the measurements were made. The temperature of the ground (absorber) was also found to drop to this value. This equation can be used to estimate the ground temperature at higher solar insolations that are experienced in the region. Interestingly, the maximum solar insolation still reached close to 1000 W/m^2 during the months of May to October as well while the maximum temperature reached close to 304 K. The variation in the mean solar insolation in different months in Fiji and other PICs is small, as these countries are close to the equator [60].

The temperature rise of air along the collector recorded every two hours from 9.00 am to 9.00 pm on a day when the maximum solar insolation crossed 1000 W/m^2, are shown in Fig. 21. The gradual increase in temperature from the collector inlet to the center can clearly be seen at all the times of the day. The temperature rise is the highest at 1.00 pm, at which time the solar insolation was also the highest. The collector air temperatures drop a little at 2.00 pm and a little more at 3.00 pm. The temperatures are significantly lower at 11.00 am and then at 5.00 pm. As expected, the temperatures were the lowest at 9.00 pm. In this month, the sunset time is about 6.45 pm, so the collector was not receiving any sunlight at 7.00 pm and 9.00 pm. However, the collector air temperatures are higher than the ambient temperature and continue to rise towards the center due to higher temperature of the ground under the collector. At 9.00 pm, the temperature rise is too small which results in a small velocity of air in the chimney, as shall be seen later. The maximum temperature rise above the ambient temperature is more than 24 degrees, as can be seen from the figure.

The temperature rise along the collector from the inlet to the center was measured on different days and times when the solar

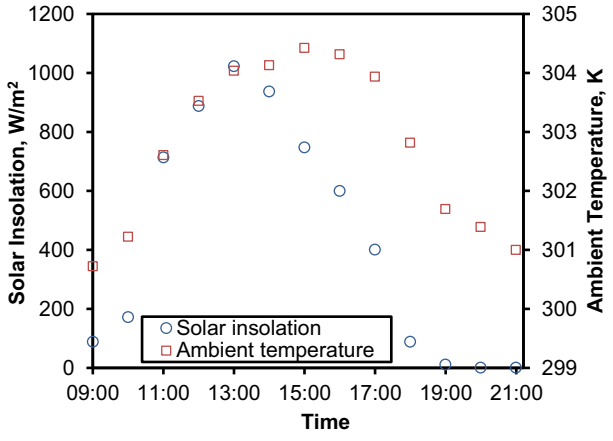

Fig. 19. Variations of solar insolation and ambient temperature averaged over three typical days in February 2016. The maximum deviation in solar insolation from the averaged values was 205 W/m^2 and that in the temperature was 2 K.

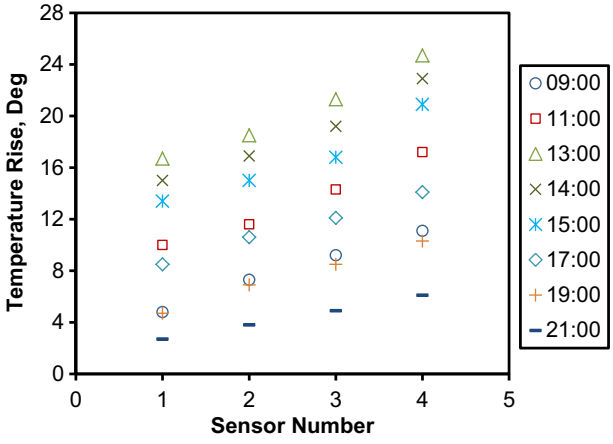

Fig. 21. Temperature rise of air from the inlet to the center of the collector measured every two hours from 9.00 am to 9.00 pm.

insolations were different. The variation in temperature rise is shown in Fig. 22. As can be seen from the figure, the solar insolation varied from 366 W/m^2 to 1007 W/m^2. Extreme care was taken for recording these temperature readings. It was ensured that the direct sunlight was continuously falling on the system for at least half-an-hour before the measurements were recorded and saved. Sensor number 4 recorded the maximum temperature rise of 21.8 degrees at the time of maximum solar insolation of 1007 W/m^2. For their Type I collector, Pasumarthi and Sherif [16] reported a temperature rise of about 14 degrees at a solar insolation of 826 W/m^2, while it is 18 degrees in the present work.

The temperature variations were also measured along the height of the chimney on the same day on which the measurements reported in Fig. 21 were performed. The temperatures along the chimney height were generally found to decrease slightly, as can be seen from Fig. 23. The temperature rise (difference) compared to the ambient temperature is the highest at 1.00 pm. At 1.00 pm, some of the sun's rays were directly entering the opening at the top of the chimney, hence the temperature at sensor number 7 probably dropped very little compared to the temperature at sensor number 6. A comparison of the temperatures in Fig. 21 and Fig. 23 shows that the temperature drops by about 2–3 degrees from sensor number 5 to sensor number 7 throughout the day except for 9.00 pm when the temperature rise (Fig. 21) as well as the temperature drop were relatively small.

Measurements of air velocity were performed inside the chimney at the throat (shown in Fig. 7) by measuring the difference in total and static pressures with a Pitot static tube at different times of the day and at different solar insolations. Fig. 24 shows the hourly variation of the air velocity from 9.00 am to 9.00 pm performed for two different days with solar insolations similar to those shown in Fig. 19. The air velocities were below 2 m/s at 9.00 am and 10.00 am but increased significantly at 11.00 am and reached a maximum at 1.00 pm. Almost all the times when air velocity measurements were performed, it was observed that the peak velocity is recorded at 1.00 pm. This is interesting because the ambient temperature peaked at 2.00 pm or 3.00 pm most of the days round the year. The maximum air velocity was about 5.4 m/s which corresponded to the solar insolation greater than 1000 W/m^2. The air velocities after 10.00 pm were very small. This is contrary to the results of numerical simulation presented by Schlaich [4] which showed power production of about 10% at night time without water storage. This is due to the small size of the collector in the present work, causing the ground to loose heat quickly due to convection.

The air velocities at the chimney throat were measured on different days at a number of solar insolations above 200 W/m^2 and

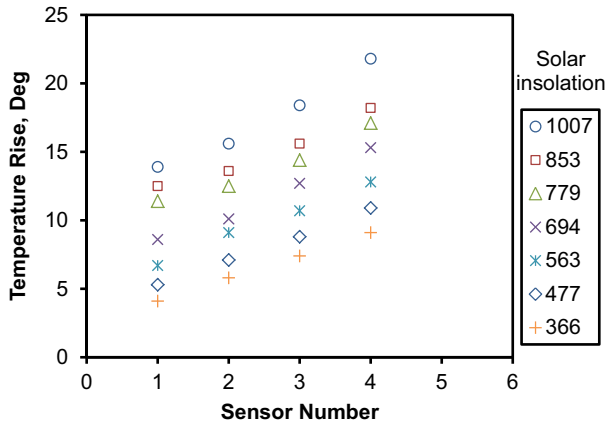

Fig. 22. Temperature rise of air inside the collector at different solar insolations.

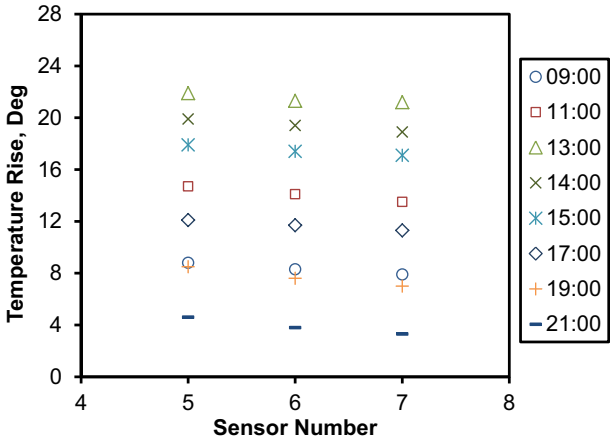

Fig. 23. Temperature rise of air along the chimney height measured every two hours from 9.00 am to 9.00 pm.

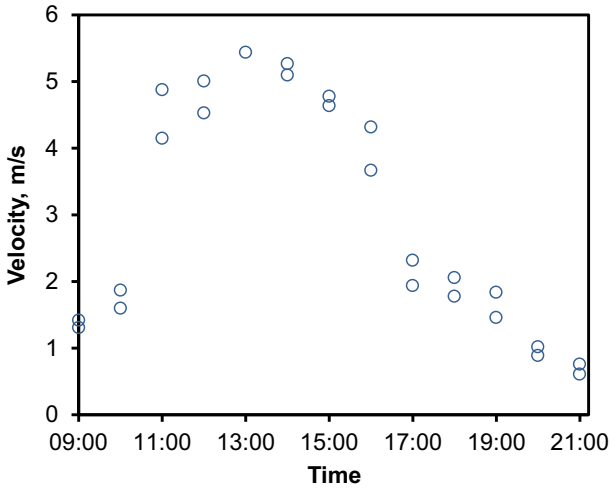

Fig. 24. Variations of air velocity at the turbine section from 9.00 am to 9.00 pm.

the results are plotted in Fig. 25. The figure shows a wide scatter in the air velocities. The velocities that were significantly different from the ones plotted were not considered, as those were mainly either due to non-zero atmospheric wind or due to the ground temperature being significantly different from the values plotted in Fig. 20. It was also due to the fact that the ground and collector temperatures were not the same during morning and evening times even though the solar insolations were similar; this is expected because the ground gets heated up slowly as the day progresses and the afternoon ground and collector temperatures were higher compared to morning temperatures. The linear best-fit obtained from the graph is represented by the equation

$$y = 0.0051x + 0.47 \quad (5)$$

Air velocities at the chimney throat at different solar insolations were estimated based on the linear Eq. (5) and the power available to the turbine was estimated using Eq. (3). Fig. 26 shows the variation of the power with solar insolation. It can be seen that the power available increases about 5 times when the solar insolation is doubled from 500 W/m^2 to 1000 W/m^2.

5.4. Effect of atmospheric wind

It was observed at a number of times during the present work that the atmospheric wind increases the air velocity at the chim-

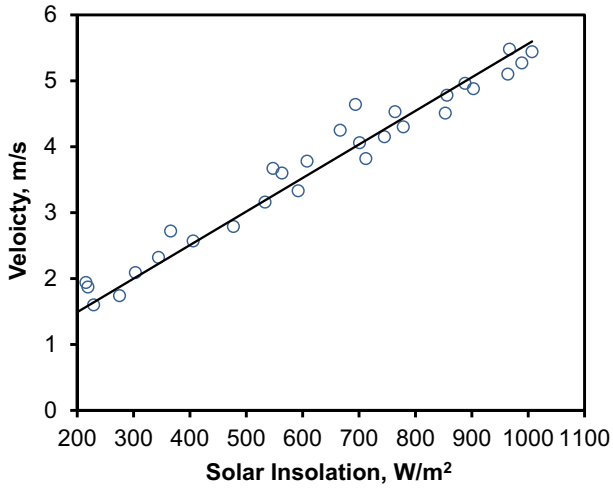

Fig. 25. Variation of air velocity in the turbine section with solar insolation.

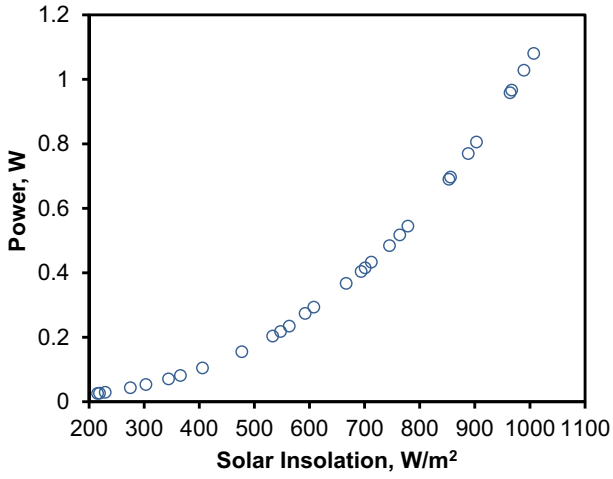

Fig. 26. Variation of power available to the turbine with solar insolation.

ney throat. On the other hand, it has been reported in the literature [43,47,61] that atmospheric wind reduces the air velocity through the turbine and hence the power available. This is especially the case for higher collector inlet openings, as the heated air under the collector gets blown away by the entering atmospheric wind, reducing the temperature difference that drives the air through the chimney and hence the buoyancy effect [47]. The effect of atmospheric wind was investigated at two solar insolations and five wind speeds. The wind speed was measured at a height of about 2 m above the ground level with a pitot static tube. Fig. 27 shows the variation of air velocity at the turbine section of the SCPP with atmospheric wind at the solar insolations of 547 W/m^2 and 829 W/m^2. It can be seen that the air velocity in the turbine section increases with increasing atmospheric wind. Above a wind speed of 4 m/s, the rate of increase of air velocity in the SCPP is lower compared to lower wind speeds.

This opposite effect observed in the present work compared to the previously reported effect is probably due to the small collector inlet opening. It was observed that the ground temperature as well as the air temperature under the collector reduce by 2–4 degrees in the presence of wind (not shown) on the side of the collector from where the wind is flowing. However, the entrainment of the air exiting the chimney by the cross-wind results in drawing of more air from the chimney, increasing the air velocity in the turbine

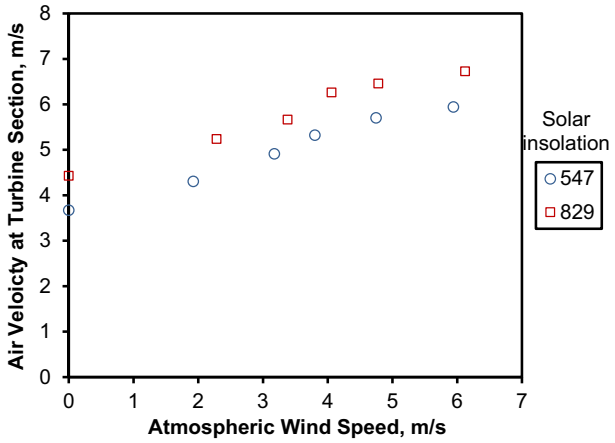

Fig. 27. Effect of atmospheric wind on the air velocity at the turbine section.

section and hence the available power. The small collector opening, which also acts as exit for the atmospheric wind, does not take a large amount of wind and also makes it difficult for the wind to exit from the opposite end because of the constriction type of geometry. The suction effect from the top of the chimney is apparently higher compared to the pressure difference developed inside, that causes the flow to exit from the smaller exit area. It was found in the previous works [47,61] that smaller collector inlet is better when it comes to the adverse effect of cross-wind as it does not allow carrying away of the heated air from the other end. Findings from the present and the above previous works suggest that there could be an optimum collector inlet opening for a given SCPP that will not experience any gain or loss of available power in the presence of atmospheric wind and the system will perform as per the design.

5.5. Effect of water bags

Normally, it is expected that a practical SCPP provides power round the clock. The concept of heat storage in water bags has been used by researchers to accomplish this [4,43]. The water bags receive heat in the daytime and release it at night time when the solar energy is not available. To investigate the process of heat storage in water bags during the day and of heat release from the bags during the night, 32 water bags, each of dimensions 220 mm × 160 mm × 50 mm and a capacity of about 1.7 L were placed under the collector. The water bags occupied an area of 14% of the total collector area. The experiments were carried out in the month of March 2016 when the ambient temperatures start dropping. Fig. 28 shows the typical solar insolation and ambient temperature for this month. It can be seen that the temperatures as well as solar insolations are slightly lower compared to the month of February. The maximum solar insolation, however, still reached close to 1000 W/m^2. This was also recorded at 1.00 pm.

The water bag temperature was measured along with the ground temperature at different solar insolations. It was found that the ground temperatures are still comparable to the case when no water bags were deployed. The highest temperature of the water bag was recorded at an insolation of 955 W/m^2 at 340 K, which is about the same as the ground temperature at that insolation (Fig. 20). However, generally, the water bag temperature was found be lower by 2–5 degrees compared to the ground temperature in the day time. The temperature of water inside the bags was found to be lower than the bag temperature by 2 or 3 degrees during the day time; however, at night time, the water bag temperature was found to be slightly lower compared to the water

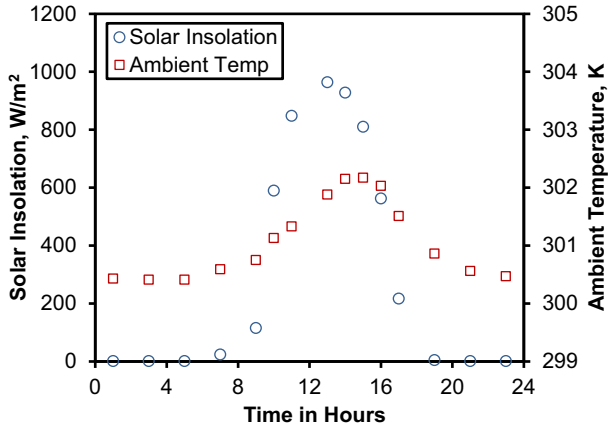

Fig. 28. Variations of solar insolation and ambient temperature averaged over three days in March 2016. The maximum deviation in solar insolation from the averaged values was 165 W/m^2 and that in the temperature was 2 K.

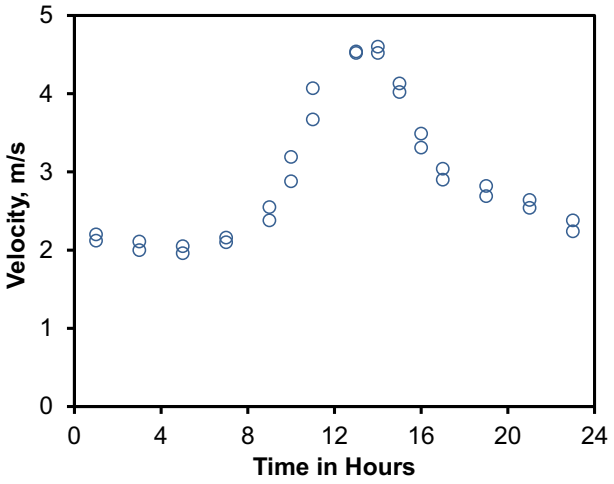

Fig. 30. Diurnal variation of air velocity at the turbine section.

temperature. Fig. 29 shows the diurnal variation of the water bag temperature. Similar trend was reported by Larbi et al. [43]. It is interesting to observe that the maximum water bag temperature coincided with the peak solar insolation – both occurring at 1.00 pm. However, the water bag temperature remained high for the next two hours as can be seen from Fig. 29. The bag temperature dropped considerably at 4.00 pm mainly due to a significant drop in solar insolation. However, the water bag temperature dropped by only about 6 degrees at night time. The figure also shows the water bag temperature relative to the ambient temperature. It can be seen that the water bag temperature was greater than the ambient temperature round the clock with the minimum difference being about 11 degrees. This gave rise to a continuous flow of air through the chimney, as shown in Fig. 30.

Fig. 30 shows the diurnal variation of air velocity at the throat (turbine section) on two similar days. As mentioned earlier, when the water bags were placed under the collector, a continuous flow of air was observed at the turbine section. The maximum velocities were recorded at 1.00 pm and 2.00 pm. The velocities start reducing after that. There is a significant drop in air velocity after 5.00 pm. However, after the sunset, the air continues to flow through the chimney due to the heat release from the water bags. At 9.00 pm, the air velocity is above 2 m/s in the presence of water bags. A comparison with Fig. 24 shows a significant difference due to the water bags at this time. As the water bag temperature continues to drop after 9.00 pm, the air velocity at the throat also continues to drop. The minimum velocity is recorded at 5.00 am at which time the water bag temperature is also the lowest. The velocity then starts to increase as the sun rises and heat is received by the absorber.

It should be noted that the maximum air velocity in the presence of water bags is lower compared to that in the absence of water bags (Fig. 24). This is mainly because some of the heat is getting stored in the water bags in the daytime reducing the heating of the air under the collector. Fig. 31 shows the power available at the chimney throat with and without water bags for the 24 h. The power available at the peak time of 1.00 pm in the presence of water bags is about 60% of that in the absence of the bags, which is similar to the results presented in Ref. [4]. However, the power available at night time is much less compared to Ref. [4], but is comparable to the results presented by Larbi et al. [43]. The average power available to the turbine during zero-insolation hours is 14.3% of the peak power. The total energy of the plant in 24 h with the water bags is 13.9% less than that without the water bags. There is a possibility of the water bags close to the collector inlet losing some heat to the air adjacent to the collector, resulting in some loss of energy; however, the bags ensure round-the-clock availability of energy from the SCPP. It can also be seen from the Fig. 31 that the power varies significantly from daytime to nighttime. Guo et al. [62] studied the performance of an SCPP with heat storage using different types of soils with steady and unsteady the-

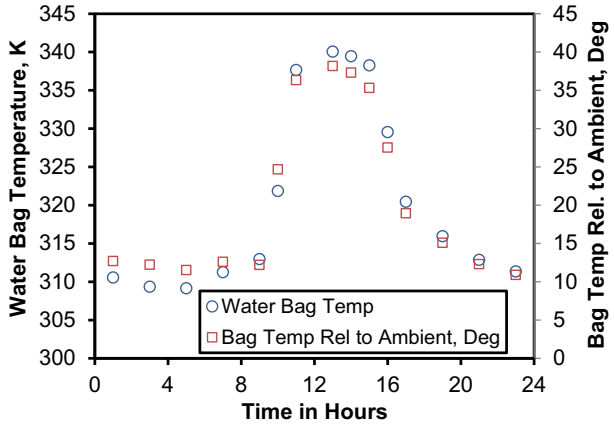

Fig. 29. Diurnal variation of water bag temperature.

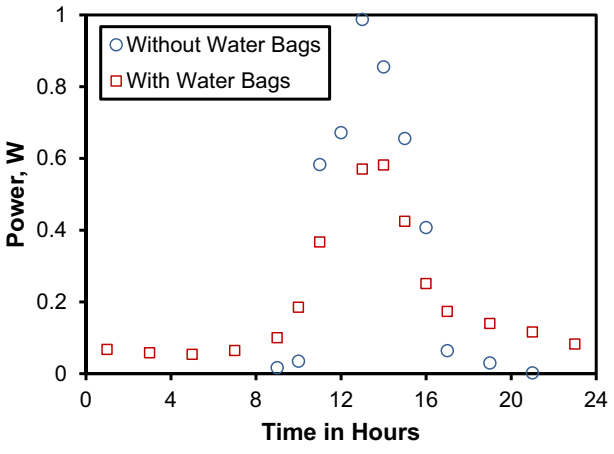

Fig. 31. Diurnal variation of power available at the turbine section with and without water bags.

oretical models. They found that with increasing specific heat capacity of soil, the fluctuation in power output will be less. They observed that the fluctuation factor (ratio of the power output at different times of the day to the minimum power output of the day) depends on the thermal inertia which is defined as the square root of the product of the thermal conductivity and volumetric heat capacity of a material, and is a measure of the resistance of the material to temperature change. The maximum fluctuation factor in their studies varied from 4.75 to 14. In the present work, the maximum fluctuation factor was 10.8; however, the maximum fluctuation factor during zero-solar insolation hours was only 2.59 indicating that water can be used as an effective heat storage medium. The transient effect can be reduced by providing more water bags.

5.6. Simulation of 100 m tall SCPP

CFD simulations were performed for the 100 m tall SCPP. A 10:1 scaled up model of the 10 m SCPP was simulated and the results are presented and discussed in this section. Partial geometric similarity between the 10 m SCPP and the 100 m SCPP was maintained which, for an overall height of 100 m gave a collector diameter of 80 m. The inlet opening of the collector was 0.5 m and the outlet height of the collector was 5 m. The collector outlet diameter was 10 m and the chimney throat diameter was 2.5 m. The chimney divergence angle was kept the same at 2°. The solar insolation and ground temperature were 607.8 W/m^2 and 323 K respectively for the simulations. More accurate values of available power will be obtained if the variation of ground temperature in the radial direction due to convection between the ground and the air is taken into consideration.

The temperature variation along the height of the chimney is shown in Fig. 32. The temperature dropped by about 16 degrees from the collector outlet to the top of the chimney.

The variation of the velocity along the height of the chimney is shown in Fig. 33. The velocity increases sharply until the chimney throat and then starts to decrease as the cross-sectional area of the tower increases due to the divergent chimney. A maximum velocity of 22.72 m/s was recorded for this SCPP at the solar insolation of 607.8 W/m^2. The mass flow rate through the chimney was 137.31 kg/s. Koonsrisuk and Chitsomboon [63] also reported similar trends for a similar sized tower.

This SCPP design gave a maximum available power exceeding 35 kW at this solar insolation. Using the slope of eqn. (5), the velocities at the turbine section were estimated for different solar insolations and the available power was estimated. It should be noted that the solar insolation is very high in the PICs. For example, the maximum solar insolation recorded in Kiribati and Nauru was above 1330 W/m^2 in 2013–2016. Interestingly, at these two places where we collected solar insolation data, the peak insolation is above 1000 W/m^2 on a number of days round the year [60]. Even in Fiji, the maximum insolations recorded in January, November and December 2015/2016 were above 1050 W/m^2. Past works have shown that there is a significant increase in collector temperature, air velocity through the chimney and hence the power when the solar insolation is high [8,9,16,30]. The power available at different solar insolations for this 100 m high SCPP is shown in Fig. 34. At the solar insolation of 1300 W/m^2, the available power exceeds 50 kW. The annual mean daytime solar insolation in Fiji is above 300 W/m^2, while that in Kiribati is above 400 W/m^2 [60], making it possible to generate a mean annual power of 25 kW and above with a single 100 m high SCPP. The findings from the effect of water bags in Section 5.4 and the performance of a 100 m high SCPP at different solar insolations found in the PICs fills some of the gaps identified in the comprehensive review carried out by Kasaeian et al. [64].

In view of these, SCPP are very appropriate for meeting the power requirements of small islands in PICs where the requirements are of the order of tens of kiloWatts. More than half of the area on most of the islands is available for development.

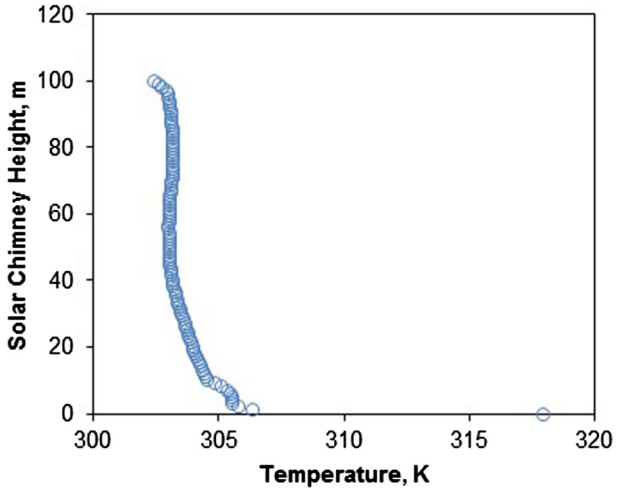

Fig. 32. Temperature variation from the collector to the top of the chimney for the 100 m SCPP.

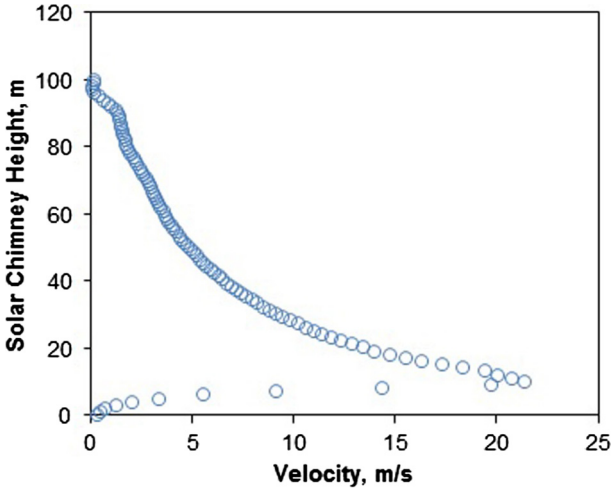

Fig. 33. Velocity variation from the bottom to the top of the chimney for the 100 m SCPP.

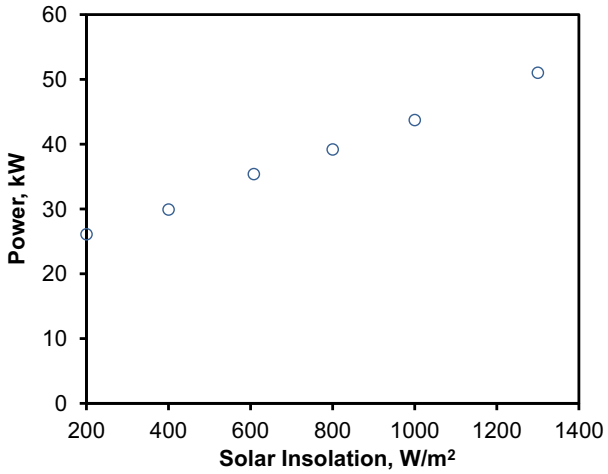

Fig. 34. Power available for the 100 m tall SCPP at different solar insolations.

6. Conclusions

Various geometric parameters of an SCPP were varied first for a 10 m high SCPP. Smaller collector inlet openings result in a better performance than larger collector openings. The collector outlet height is also a very important parameter; it is required to find an optimum height through computations to obtain the best performance from an SCPP. Other important parameters are the collector outlet diameter and the chimney throat diameter. The divergent chimney with an angle of 2° was found to perform better than a cylindrical one. Based on the findings from the 10 m SCPP, a 4 m SCPP was tested – first computationally by varying the collector outlet diameter and the chimney throat diameter. Based on the best configuration obtained from the CFD work, an experimental model was built and tested. The ground temperature was measured at different solar insolations and a mathematical correlation between the two was obtained. The temperature rise of the air inside the collector was studied as a function of solar insolation. The air velocity at the chimney throat was measured at different times of the day as well as at different solar insolations and a mathematical correlation between the two is obtained. It was also found that atmospheric wind increases the airflow through the chimney. Water bags covering an area of 14% of the area under the collector ensured that continuous round the clock power can be produced; however, the available power during the 24 h period still varied indicating that more water bags would reduce the fluctuations. Finally, a 100 m tall SCPP was modeled and tested computationally; it can give mean (annual) power of more than 25 kW and of more than 50 kW at the solar insolation of 1300 W/m^2. Such SCPPs can really help the PICs in meeting their energy requirements.

References

[1] Energy Information Administration. International energy outlook 2016. Report No. DOE/EIA-0484(2016). USA.

[2] Zhou X, Yang J, Xiao B, Hou G, Xing F. Analysis of chimney height for solar chimney power plant. Appl Therm Eng 2009;29:178–85. http://dx.doi.org/10.1016/j.applthermaleng.2008.02.014.

[3] Patel SK. Computational and experimental studies on a solar chimney power plant MSc Thesis. Fiji: The University of the South Pacific, Suva; 2013.

[4] Schlaich J, Bergermann R, Schiel W, Weinrebe G. Design of commercial solar updraft tower systems – utilization of solar induced convective flows for power generation. ASME J Sol Energy Eng 2005;127:117–25. http://dx.doi.org/10.1115/1.1823493.

[5] Bernardes MAdS, Vob A, and Weinrebe G. Thermal and technical analyses of solar chimneys. Solar Energy, 2003;75, 511–524.

[6] Hamdan MO. Analysis of a solar chimney power plant in the Arabian Gulf region. Renew Energy 2011;36:2593–8. http://dx.doi.org/10.1016/j.renene.2010.05.002.

[7] Pasumarthi N, Sherif SA. Experimental and theoretical performance of a demonstration solar chimney model - Part1: mathematical model development. Int J Energy Res 1998;22:277–88.

[8] Guo P, Li J, Wang Y, Wang Y. Numerical study on the performance of a solar chimney power plant. Energy Convers Manage 2015;105:197–205. http://dx.doi.org/10.1016/j.enconman.2015.07.072.

[9] Zhou X, Xu Y. Solar updraft tower power generation. Sol Energy 2016;128:95–125. http://dx.doi.org/10.1016/j.solener.2014.06.029.

[10] Haaf W, Friedrich K, Mayr G, Schlaich J. Solar chimneys, Part I: principle and construction of the pilot plant in manzanares. Int J Sol Energy 1983;2:3–20.

[11] Haaf W. Solar towers, Part II: preliminary test results from the Manzanares pilot plant. Int J Sol Energy 1984;2:141–61.

[12] Schlaich J. The Solar chimney. Stuttgart, Germany: Edition Axel Menges; 1995.

[13] Bernardes MAdS, Valle RM, Cortez MF. Numerical analysis of natural laminar convection in a radial solar heater. Int J Thermal Sci. 1999, 38, 42–50. http://dx.doi.org/10.1016/S0035-3159(99)80015-4.

[14] Padki MM, Sherif SA. Solar chimney for medium-to-large scale power generation. In: Proceedings of the Manila international symposium on the development and management of energy resources. Manila, Philippines, 1989, vol. 1, 432–437.

[15] Padki MM, Sherif SA. Solar chimney for power generation in rural areas. in: Seminar on energy conservation and generation through renewable resources. Ranchi, India, 1989, 91–96.

[16] Pasumarthi N, Sherif SA. Experimental and theoretical performance of a demonstration solar chimney model – part II: experimental and theoretical results and economic analysis. Int J Energy Res 1998;22:443–61.

[17] Kroger DG, Blaine D. Analysis of the driving potential of a solar chimney power plant. Research and Development J, South African Institute of Mechanical Engineers 1999;15:85–94.

[18] Ming T, Liu W, Xu G. Analytical and numerical investigation of the solar chimney power plant systems. Int J Energy Res 2006;30:861–73. http://dx.doi.org/10.1002/er.1191.

[19] Pretorius JP, Kroger DG. Thermo-economic optimization of a solar chimney power plant. Paper presented at the CHISA 2006–17th International Congress of Chemical and Process Engineering, Prague, 2006.

[20] Pastohr H, Kornadt O, Gurlebeck K. Numerical and analytical calculations of the temperature and flow field in the upwind power plant. Int J Energy Res 2004;28:495–510. http://dx.doi.org/10.1002/er.978.

[21] Huang H, Zhang H, Huang Y, Lu F. Simulation calculation on solar chimney power plant system. In: Cen K, Chi Y, Wang F, editors. Challenges of power engineering and environment 2007: 1158–1161. Berlin, Heidelberg: Springer. http://dx.doi.org/10.1007/978-3-540-76694-0_216.

[22] Ming T, Liu W, Pan Y, Xu GL. Numerical analysis of flow and heat transfer characteristics in solar chimney power plants with energy storage layer. Energy Convers Manage 2008;49:2872–9. http://dx.doi.org/10.1016/j.enconman.2008.03.004.

[23] Koonsrisuk A, Chitsomboon T. A single dimensionless variable for solar chimney power plant modelling. Sol Energy 2009;83:2136–43. http://dx.doi.org/10.1016/j.solener.2009.07.015.

[24] Ming T, Zheng Y, Liu C, Liu W, Pan Y. Simple analysis on thermal performance of solar chimney power generation systems. J Energy Inst 2010;83:6–11. http://dx.doi.org/10.1179/014426009X12519696923902.

[25] Zhou X, Wang F, Ochieng RM. A review of solar chimney power technology. Renew Sustain Energy Rev 2010;14:2315–38. http://dx.doi.org/10.1016/j.rser.2010.04.018.

[26] Sangi R, Amidpour M, Hosseinizadeh B. Modeling and numerical simulation of solar chimney power plants. Sol Energy 2011;5:829–38. http://dx.doi.org/10.1016/j.solener.2011.01.011.

[27] Xu GL, Ming T, Pan Y, Meng FL, Zhou C. Numerical analysis on the performance of solar chimney power plant system. Energy Convers Manage 2011;52:876–83. http://dx.doi.org/10.1016/j.enconman.2010.08.014.

[28] Kratzig WB. Physics, computer simulation and optimization of thermo-fluidmechanical processes of solar updraft power plants. Sol Energy 2013;98:2–11. http://dx.doi.org/10.1016/j.solener.2013.02.017.

[29] Fasel HF, Meng FL, Shams E, Gross A. CFD analysis for solar chimney power plants. Sol Energy 2013;98:12–22. http://dx.doi.org/10.1016/j.solener.2013.08.029.

[30] Koonsrisuk A, Chitsomboon T. Mathematical modeling of solar chimney power plants. Energy 2013;51:314–22. http://dx.doi.org/10.1016/j.energy.2012.10.038.

[31] Koonsrisuk A, Chitsomboon T. Effects of flow area changes on the potential of solar chimney power plants. Energy 2013;51:400–6. http://dx.doi.org/10.1016/j.energy.2012.12.051.

[32] Gholamalizadeh E, Mansouri SH. A comprehensive approach to design and improve a solar chimney power plant: A special case – Kerman project. Appl Energy 2013;102:975–82. http://dx.doi.org/10.1016/j.apenergy.2012.06.012.

[33] Chan CY, Hu SY, Raynal M, Leung YC, Chang APS, Yao JB. A telescopic divergent chimney for power generation based on forced air movement: Principle and theoretical formulation. Appl Energy 2014;136:873–80. http://dx.doi.org/10.1016/j.apenergy.2014.04.086.

[34] Li Y, Liu S. Experimental study on thermal performance of a solar chimney combined with PCM. Appl Energy 2014;114:172–8. http://dx.doi.org/10.1016/j.apenergy.2013.09.022.

[35] Patel SK, Prasad D, Ahmed MR. Computational studies on the effect of geometric parameters on the performance of a solar chimney power plant. Energy Convers Manage 2014;77:424–31. http://dx.doi.org/10.1016/j.enconman.2013.09.056.

[36] Zhou XP, Yang JK, Xiao B, Hou GX. Experimental study of the temperature field in a solar chimney power setup. Appl Therm Eng 2007;27:2044–50. http://dx.doi.org/10.1016/j.applthermaleng.2006.12.007.

[37] Ketlogetswe C, Fiszdon JK, Seabe OO. Solar chimney power generation project-the case for Botswana. Renew Sustain Energy Rev 2008;12:2005–12. http://dx.doi.org/10.1016/j.rser.2007.03.009.

[38] Maia CB, Ferreira AG, Valle RM, Cortez MFB. Analysis of the airflow in a prototype of a solar chimney dryer. Heat Transfer Eng 2009;30:393–9. http://dx.doi.org/10.1080/01457630802414797.

[39] Motoyama M, Ohya Y, Karasudani T, Nagai T, Okada S, Sugitani K. Improving the power generation performance of a solar tower using thermal updraft wind. Energy and Power Eng 2014;6:362–70. http://dx.doi.org/10.4236/epe.2014.611031.

[40] Lee DS, Hung TC, Lin JR, Zhao J. Experimental investigations on solar chimney for optimal heat collection to be utilized in organic Rankine cycle. Appl Energy 2015;154:651–62. http://dx.doi.org/10.1016/j.apenergy.2015.05.079.

[41] Maghrebi MJ, Nejad RM, Masoudi S. Performance analysis of sloped solar chimney power plants in the southwestern region of Iran. Int J Ambient Energy 2016:1–8. http://dx.doi.org/10.1080/01430750.2016.1155487.

[42] Semai H, Bouhdjar A, Larbi S. Canopy slope effect on the performance of the solar chimney power plant. Int J Green Energy 2016;14:229–38. http://dx.doi.org/10.1080/15435075.2016.1253580.

[43] Larbi S, Bouhdjar A, Meliani K, Taghourt A, Semai H. Solar chimney power plant with heat storage system performance analysis in South Region of Algeria. Proceedings of 3rd International Renewable and Sustainable Energy Conference (IRSEC) 2015: http://dx.doi.org/10.1109/IRSEC.2015.7454948.
[44] Okaye CO, Taylan O. Performance analysis of a solar chimney power plant for rural areas in Nigeria. Renew Energy 2017;104:96–108. http://dx.doi.org/10.1016/j.renene.2016.12.004.
[45] Okaye CO, Solyali O, Taylan O. A new economic feasibility approach for solar chimney power plant design. Energy Convers Manage 2016;126:1013–27. http://dx.doi.org/10.1016/j.enconman.2016.08.080.
[46] Guo P, Wang Y, Meng Q, Li J. Experimental study on an indoor scale solar chimney setup in an artificial environment simulation laboratory. Appl Therm Eng 2016;107:818–26. http://dx.doi.org/10.1016/j.applthermaleng.2016.07.025.
[47] Ming T, Wu Y, de-Richter RK, Liu W, Sherif SA. Solar updraft power plant system: A brief review and a case study on a new system with radial partition walls in its collector. Renew Sustain Energy Rev 2017;69:472–87. http://dx.doi.org/10.1016/j.rser.2016.11.135.
[48] Koonsrisuk A. Analysis of flow in solar chimney for an optimal design purpose. Ph.D. thesis, Suranaree University of Technology, Nakhon Ratchasima, Thailand, 2009.
[49] Ghorbani B, Ghashami M, Ashjaee M, Hosseinzadegan H. Electricity production with low grade heat in thermal power plants by design improvement of a hybrid dry cooling tower and a solar chimney concept. Energy Convers Manage 2015;94:1–11. http://dx.doi.org/10.1016/j.enconman.2015.01.044.
[50] Hu S, Leung DYC, Chan JCY. Impact of the geometry of divergent chimneys on the power output of a solar chimney power plant. Energy 2017;120:1–11. http://dx.doi.org/10.1016.j.energy.2016.12.098.
[51] Ali B. Techno-economic optimization for the design of solar chimney power plants. Energy Convers Manage 2017;138:461–73. http://dx.doi.org/10.1016/j.enconman.2017.02.023.
[52] Ayadi A, Driss Z, Bouabidi A, Abid MS. Experimental and numerical study of the impact of the collector roof inclination on the performance of a solar chimney power plant. Energy and Buildings 2017;139:263–76. http://dx.doi.org/10.1016/j.enbuild.2017.01.047.
[53] Shirvan KM, Mirzakhanlari S, Mamourian M, Kalogirou SA. Optimization of effective parameters on solar updraft tower to achieve potential maximum power output: A sensitivity analysis and numerical simulation. Appl Energy 2017;195:725–37. http://dx.doi.org/10.1016/j.apenergy.2017.03.057.
[54] Bilgen E, Rheault J. Solar chimney power plants for high latitudes. Sol Energy 2005;79:449–58. http://dx.doi.org/10.1016/j.solener.2005.01.003.
[55] ANSYS. ANSYS CFX-Solver theory guide, 2011. ANSYS Inc., Canonsburg, Pennsylvania.
[56] Moffat RJ. Describing the uncertainties in experimental results. Exp Thermal Fluid Sci 1988;1:3–17.
[57] Okada S, Uchida T, Karasudani, Ohya Y. Improvement in solar chimney power generation by using a diffuser tower. ASME J Sol Energy Eng 2015;137:031009–1-031009-8. http://dx.doi.org/10.1115/1.4029377.
[58] Shahreza AR, Imani H. Experimental and numerical investigation on an innovative solar chimney. Energy Convers Manage 2015;95:446–52. http://dx.doi.org/10.1016/j.enconman.2014.10.051.
[59] Lutgens FK, Tarbuck EJ. The atmosphere – an introduction to meteorology. 12th ed. USA: Pearson; 2013.
[60] Aukitino T. Assessment of renewable energy resources in Kiribati MSc Thesis. Fiji: The University of the South Pacific, Suva; 2017.
[61] Shen W, Ming T, Ding Y, Wu Y, de_Richter RK. Numerical analysis on an industrial-scaled solar updraft power plant system with ambient crosswind. Renew Energy 2014;68:662–76. http://dx.doi.org/10.1016/j.renene.2014.03.011.
[62] Guo P, Wang Y, Li JY, Wand Y. Thermodynamic analysis of s solar chimney power plant system with soil heat storage. Appl Therm Eng 2016;100:1076–84. http://dx.doi.org/10.1016/j.applthermaleng.2016.03.008.
[63] Koonsrisuk A, Chitsomboon T. Effect of tower area change on the potential of solar tower. In: Proceedings of the 2nd Joint International Conference on Sustainable Energy and Environment (SEE 2006), Bangkok, Thailand, 2006, 1–6.
[64] Kasaeian AB, Molana S, Rahmani K, Wen D. A review on solar chimney systems. Renew Sustain Energy Rev 2017;67:954–87. http://dx.doi.org/10.1016/j.rser.2016.09.081.